Journal of Medicinal Chemistry



Article

# Discovery of Fragment-Derived Small Molecules for In Vivo Inhibition of Ketohexokinase (KHK)

Kim Huard, Kay Ahn, Paul A. Amor, David A. Beebe, Kris A Borzilleri, Boris A. Chrunyk, Steven B. Coffey, Yang Cong, Edward L. Conn, Jeffrey S. Culp, Matthew S. Dowling, Matthew F. Gorgoglione, Jemy A. Gutierrez, John D. Knafels, Erik A. Lachapelle, Jayvardhan Pandit, Kevin D. Parris, Sylvie Perez, Jeffrey A. Pfefferkorn, David A. Price, Brian Raymer, Trenton T. Ross, Andre Shavnya, Aaron C. Smith, Timothy A. Subashi, Gregory Tesz, Benjamin A. Thuma, Meihua Tu, John D. Weaver, Yan Weng, Jane M. Withka, Gang Xing, and Thomas V Magee

*J. Med. Chem.*, **Just Accepted Manuscript** • DOI: 10.1021/acs.jmedchem.7b00947 • Publication Date (Web): 30 Aug 2017



ACS Publications

Journal of Medicinal Chemistry is published by the American Chemical Society. 1155 Sixteenth Street N.W., Washington, DC 20036

# Discovery of Fragment-Derived Small Molecules for In Vivo Inhibition of Ketohexokinase (KHK)

*Kim Huard,[◊*] Kay Ahn,[⊥†] Paul Amor,[⊥] David A. Beebe,[⊥] Kris A. Borzilleri,[‖] Boris A. Chrunyk,[‖] Steven B. Coffey,[‡] Yang Cong,[‡] Edward L. Conn,[‡] Jeffrey S. Culp,[‡] Matthew S. Dowling,[‡] Matthew F. Gorgoglione,[⊥] Jemy A. Gutierrez,[⊥] John D. Knafels,[‖] Erik A. Lachapelle,[‡] Jayvardhan Pandit,[‖] Kevin D. Parris,[‖] Sylvie Perez,[⊥] Jeffrey A. Pfefferkorn,[⊥] David A. Price,[◊] Brian Raymer,[◊] Trenton T. Ross,[⊥] Andre Shavnya,[‡] Aaron C. Smith,[‡] Timothy A. Subashi,[‖] Gregory Tesz,[⊥] Benjamin A. Thuma,[‡] Meihua Tu,[◊] John D. Weaver,[‡] Yan Weng,[◊] Jane M. Withka,[‖] Gang Xing[⊥], Thomas V. Magee[⊥]*

[◊]Pfizer Inc. Medicine Design, 1 Portland Street, Cambridge, Massachusetts USA 02139

[⊥]Pfizer Inc. Internal Medicine, 1 Portland Street, Cambridge, Massachusetts USA 02139

[‖]Pfizer Inc. Structural Biology and Biophysics, Eastern Point Road, Groton, Connecticut USA 06340

[‡]Pfizer Inc. Medicine Design, Eastern Point Road, Groton, Connecticut USA 06340

Ketohexokinase, Fructokinase, Fragment-based drug design, Fructose metabolism, Hepatic steatosis, Non-alcoholic steatohepatitis

ABSTRACT: Increased fructose consumption and its subsequent metabolism have been implicated in hepatic steatosis, dyslipidemia, obesity and insulin resistance in humans. Since ketohexokinase (KHK) is the principal enzyme responsible for fructose metabolism, identification of a selective KHK inhibitor may help to further elucidate the effect of KHK inhibition on these metabolic disorders. Until now, studies on KHK inhibition with small molecules have been limited due to the lack of viable in vivo pharmacological tools. Herein we report the discovery of **12**, a selective KHK inhibitor with potency and properties suitable to evaluate KHK inhibition in rat models. Key structural features interacting with KHK were discovered through fragment-based screening and subsequent optimization using structure-based drug design and parallel medicinal chemistry led to the identification of pyridine **12**.

## INTRODUCTION

Ketohexokinase (KHK) is the rate-limiting enzyme involved in fructose metabolism and catalyzes the phosphorylation of fructose to fructose-1-phosphate (F1P).[1] Human KHK (hKHK) is expressed from two alternative mRNA splice variants, encoding the two distinct enzyme isoforms KHK-A and KHK-C. The affinity and capacity of KHK-C for fructose phosphorylation is much greater than KHK-A as evidenced by a much lower $K_m$ (0.73 mM for KHK-C vs. 28.6 mM for KHK-A), greater $k_{cat}$ ($3.14 \times 10^3$ $s^{-1}$ for KHK-C vs $3.04 \times 10^2$ $s^{-1}$ for KHK-A) and a 405-fold greater overall catalytic efficiency ($4.30 \times 10^6$ $M^{-1}s^{-1}$ for KHK-C vs. $1.06 \times 10^4$ $M^{-1}s^{-1}$ for KHK-A).[2] While KHK-A is ubiquitously expressed, the expression of KHK-C is limited to the liver, kidney, and intestine – the primary sites of fructose metabolism in the body.[3]

Fructose consumption, which has increased dramatically over the last century, may be a dietary factor contributing to non-alcoholic fatty liver disease (NAFLD), dyslipidemia, obesity and insulin resistance in humans.[4] In contrast to glucose, metabolism of fructose is not regulated by feedback inhibition. As a consequence, fructose is preferentially metabolized relative to other carbohydrates, and its metabolism generates various reactive and signaling metabolites that contribute to metabolic disease progression.[5] As an example, glycolytic metabolites generated from fructose, such as glucose-6-phosphate, activate the carbohydrate response element binding protein (ChREBP), a highly lipogenic transcription factor that can promote both steatosis and insulin resistance with carbohydrate over-feeding.[5c, 6] Consequently, post-prandial hypertriglyceridemia occurs in both rodents and humans following fructose feeding due to decreased very low density lipoprotein (VLDL) clearance and enhanced de novo lipogenesis.[3, 7] In clinical studies, high fructose consumption also increased insulin resistance and hepatic steatosis.[8] Additionally, correlation studies have revealed that consumption of fructose-containing carbonated beverages is associated with NAFLD in patients who lack other features of the metabolic syndrome, indicating that fructose intake independent of metabolic disease can increase liver fat.[9] Taken together, these data suggest that increased fructose consumption promotes features of the metabolic syndrome, such as hepatic steatosis, insulin resistance and obesity.

Studies in KHK-null mice (i.e. lacking both KHK-A and -C) have previously demonstrated that KHK is required for the adverse metabolic effects of fructose. Mice lacking KHK were protected from fructose-induced hypertriglyceridemia, insulin resistance, hepatic lipid accumulation, weight gain and adiposity compared to the wild type littermate controls.[3, 10] Interestingly, KHK-

null mice are also protected from the deleterious effects of endogenously produced fructose, as they display reduced weight gain, insulin resistance and hepatic steatosis when fed a high glucose, fructose-free diet that promotes endogenous fructose synthesis, features of insulin resistance and the metabolic syndrome.[11] KHK loss of function mutations have been reported in humans and result in a benign and asymptomatic syndrome known as essential fructosuria, in which fructose from the diet results in fructose wasting in the urine.[12] On the basis of the overall data from human genetics and non-clinical studies, KHK inhibition was proposed as a potentially safe mechanism to treat metabolic diseases.

At the molecular level, KHK-C (KHK hereafter) exists as a dimer in solution[13] and has been observed to form a dimer in all published crystal structures.[14] The main structural features of the protein as well as its interactions with fructose and AMP-PNP, a non-hydrolyzable imidophosphate analogue of ATP, have been described in detail elsewhere.[14a, 14d] Key interactions are illustrated in Figure 1, which shows two orthogonal views of AMP-PNP bound to KHK. Three noteworthy features of this binding site, indicated in Figure 1, are exploited in subsequent inhibitor designs: (1) hydrogen bond between the ribose 3'-OH and the backbone carbonyl oxygen of Gly229, part of a loop (A224-A230) that forms the 'roof' of the binding pocket in this representation; (2) water molecule that makes two hydrogen bonds with AMP-PNP, and with protein backbone atoms (backbone amide of Phe245 and backbone carbonyl of Cys282); (3) section of the binding site made up of three consecutive proline residues (246-248) that we termed the 'proline-wall', forms the 'southwest' corner of the binding pocket. Three crystal structures with bound fragments that separately interact with each of these elements are shown in Figure 3.

Relative to protein kinases, the flipped orientation of the purine ring of AMP-PNP in the binding pocket is noteworthy as it offers the possibility of finding non-hinge binding inhibitors, which could avoid broad kinome activity. An unusual feature of the hKHK-C dimeric assembly is the formation of a beta-clasp at the interface, in which residues 19-33 from one subunit (designated A) form part of a beta sheet with β-strands from the other subunit (B); hence it is a pseudo-homodimer. As a result, Asp27 from monomer B (Asp27(B)) extends into the active site of monomer A within about 6Å of the bound AMP-PNP (illustrated in Figure S1), and is a feature that was exploited in inhibitor design by others (vide infra).[14b-f]

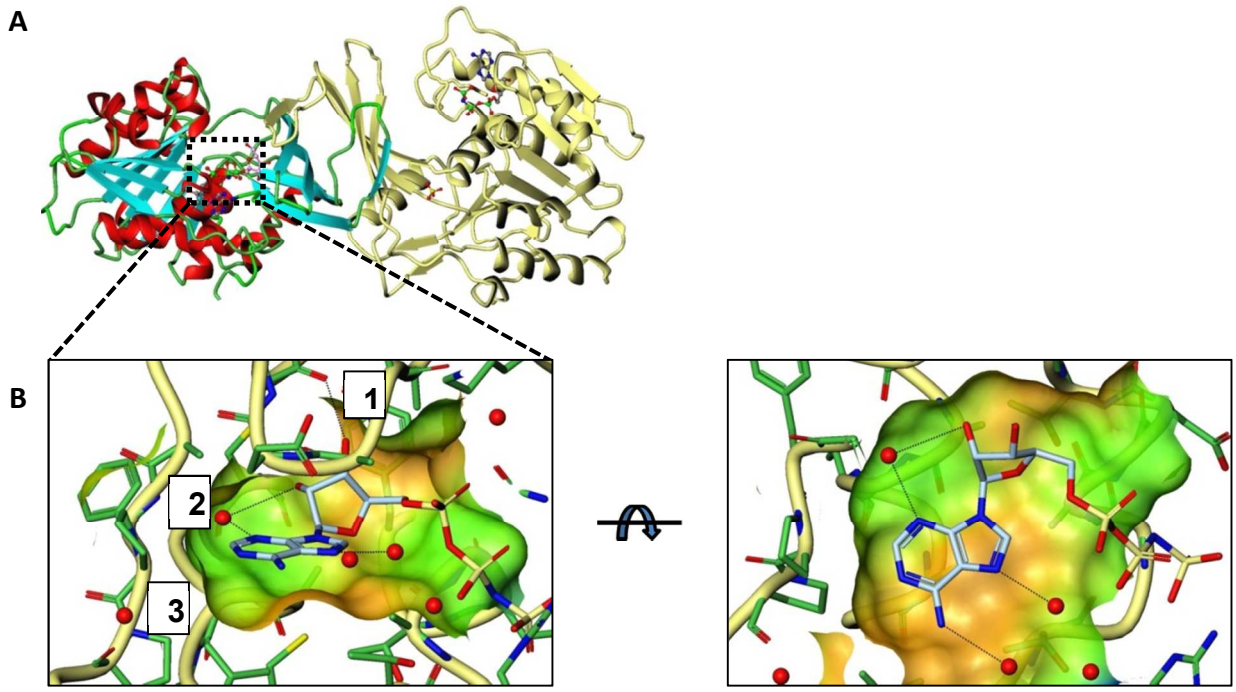


**Figure 1.** (A) hKHK-C complexed with AMP-PNP (PBD ID: 3NBV), showing the two molecules in the crystallographic asymmetric unit. Molecule A (colored by secondary structure) is in a closed conformation and Molecule B (yellow) is in an open conformation. Each molecule is bound to AMP-PNP, and the binding site in the closed conformation is shown in a close-up view in 1B. (B) A close-up view of the AMP-PNP binding site is shown in two approximately

orthogonal views. Three key interactions described in the text are identified with numbers. A semi-transparent surface is drawn around the atoms constituting the binding site, colored according to the hydrophobicity of the underlying atoms, with brown being more hydrophobic than green. Hydrogen bonds are indicated with dotted lines.

Two chemical series of hKHK inhibitors have been reported in the literature (Figure 2). A pyrimidinopyrimidine series, represented by **1**, was identified from a high throughput screening (HTS) campaign. This chemical series was optimized to provide the most potent inhibitors of hKHK reported to date. However, only low exposure levels were achieved in rat pharmacokinetic (PK) studies due to high metabolic clearance.[14b, 14c] A second series, based on an indazole core was initially identified through X-ray crystallographic fragment screening and further developed into analogs such as indazole **2** with moderate inhibitory activity against hKHK and a good rat PK profile.[14d-f] The basic amine is a key functional group in both series that specifically interact with Asp27 of monomer B as a way to improve potency in the hKHK in vitro assay.[14b-f] To our knowledge, in vitro inhibition of rodent KHK was not reported for either the pyrimidinopyrimidine or indazole series and, until now, there were no reports of in vivo KHK inhibition. In our in vitro enzymatic assays, significantly decreased potency against the rat KHK (rKHK) vs hKHK enzyme was observed for basic analogues interacting directly with Asp27(B). Comparison of the human and rat KHK amino acid sequences revealed a difference at residue 107: asparagine in human and serine in rat (Figure S1). Based on the X-ray structure, such a difference is hypothesized to create a different environment around Asp27 and cause potency shifts between species for basic compounds interacting directly with Asp27(B).

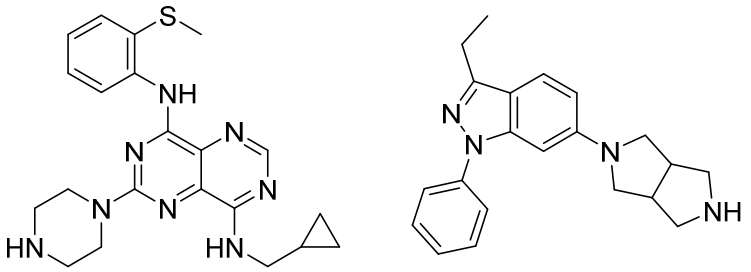


**Figure 2.** Representative structures of KHK inhibitors from the pyrimidinopyrimidine and indazole series reported in literature.

Given the limitation of the currently available KHK inhibitor tools for biological studies, we sought to identify a novel series of inhibitors that are equipotent against the human and rat KHK enzyme, with good PK properties. Fragment-based drug discovery (FBDD) is now a well-established technology for generating new chemical leads and drugs.[15] Screening of a Pfizer proprietary fragment library[16] using NMR ligand-based methods has been useful in identification of unique fragment hits for many internal targets. KHK was considered an excellent candidate for FBDD due to relatively easy generation of high quality and large quantity of a biotin acceptor peptide (BAP)-tagged stable protein for development of NMR and SPR binding assays, the precedent for robust protein crystallography, and suitable DMSO tolerance for high concentration screening. Due to prior success with our fragment library for kinases,[17] and the enabling biophysical characteristics of KHK, we initiated a FBDD approach to identify novel chemical matter. Herein we report the identification of new fragment hits from a primary ligand-based NMR screen, secondary confirmation by SPR and biochemical assays, followed by determination of key interactions observed by X-ray protein crystallography, which were then

used to rapidly provide a non-basic pharmacological tool compound for further study in rodent in vivo models.

## RESULTS AND DISCUSSION

During our search for KHK inhibitors, hKHK was screened against our previously described fragment library containing 2592 fragments using a NMR saturation transfer difference (NMR-STD) ligand-based method.[18] The total hit rate was 17%, which is consistent with other in-house NMR kinase fragment screens. Of these 451 hits, 286 (11%) were considered of high confidence based on the intensity of the NMR-STD signal. Although novel hits are generally observed for each target screened, hKHK had a significant number of unique fragment hits (11 hits, 2.4%) which were not hits in any of our 31 prior NMR fragment screens. Prior experience has taught us that application of orthogonal biophysical and biochemical assays is critical for validating fragment hits, prioritizing for X-ray crystallography, and building confidence for medicinal chemistry efforts. To this end, 448 available primary fragment hits were evaluated in an SPR binding assay using an 11 point dose response curve with a top concentration of 300 μM and two-fold dilution. Of these primary fragments hits, 114 had binding affinities ($K_D$) <100 μM while 16 fragments had $K_D$ values <25 μM.

The fragment hits were evaluated for their physicochemical properties, inhibitory activity in the KHK enzymatic assay and chemical tractability. Of the 179 SPR-validated hits, 23 were found to be functionally active in the in vitro biochemical assay ($IC_{50}$ values ranging from 46 to 439 μM) and these 23 fragments were prioritized for x-ray crystallography. Figure S2 shows that the distribution of LogD and fraction Sp3 for the selected fragments is representative of the distribution for all SPR-confirmed hits. Additionally, Figure S2 highlights the fact that the

selected fragments were neutral, which is aligned with our goal of avoiding basic amines. Finally, Figure S2 also illustrates the range of Kd covered by the selected 23 fragments, showing that not only tight binders were progressed to crystallization. All 23 fragments were found to bind in the ATP binding site with similar key interactions observed across multiple fragments. Consistent with the flipped orientation of the purine ring of ATP in this pocket relative to protein kinases, none of the hits contained a hinge-binding motif. Table 1 and Figure 3 summarize the profile and binding modes of representative hits. As mentioned previously, the hits from NMR screening were confirmed by SPR, with $K_D$ values ranging from 20 µM to 103 µM for the selected examples. Compounds **3**, **4** and **5** also showed measurable inhibitory activity in the hKHK enzymatic assay ($IC_{50}$ = 118 µM, 319 µM and 100 µM respectively).

**Table 1.** Representative hits from the NMR fragment screening

| Compound | **3** | **4** | **5** | **6** |
|---|---|---|---|---|
| | 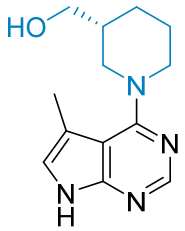 | 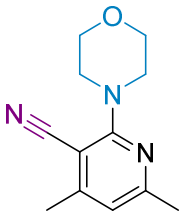 | 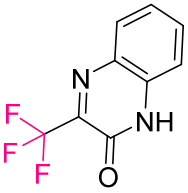 | 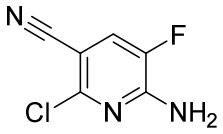 |
| $K_D$ (µM)[a] | 20 | 62 | 44 | 103 |
| hKHK $IC_{50}$ (µM)[b] | 118 | 319 | 100 | >500 |
| ($pIC_{50}$ ± SD) | (3.92 ± 0.05) | (3.50 ± 0.07) | (4.0 ± 0.3) | |
| MW[c] | 246 | 217 | 214 | 170 |
| FQ[d] | 0.53 | 0.55 | 0.50 | 0.44 |

[a]$K_D$ values were determined by SPR (n=1). [b]$IC_{50}$ values for hKHK are reported as the mean of 3 replicates with $pIC_{50}$ ± SD in parentheses. [c]MW: molecular weight. [d]FQ: fit quality is a scaled measure of ligand efficiency that centers optimal binders near 1.0.[19] The functional groups

identified in blue, purple and pink respectively make key interactions with the ribose pocket, conserved water molecule and proline wall as described in Figure 3.

Most of the confirmed hits contained a heteroaromatic core (observed in the narrow ATP binding pocket) with multiple aliphatic substituents. As exemplified by compounds **3** and **4**, saturated heterocyclic rings with polar functionalities such as an alcohol or an ether were deeply embedded in the ribose pocket (Figure 3A and B). Interestingly, a high fraction of the fragment hits contained a nitrile group. In the examples selected for crystallization, the nitrile group was found to accept a hydrogen bond with a conserved water molecule deep in the binding site (Figure 3B). Additionally, various lipophilic groups such as methyl or trifluoromethyl (in compounds **4** and **5** respectively) made hydrophobic interactions with the proline wall (Figure 3B and C).

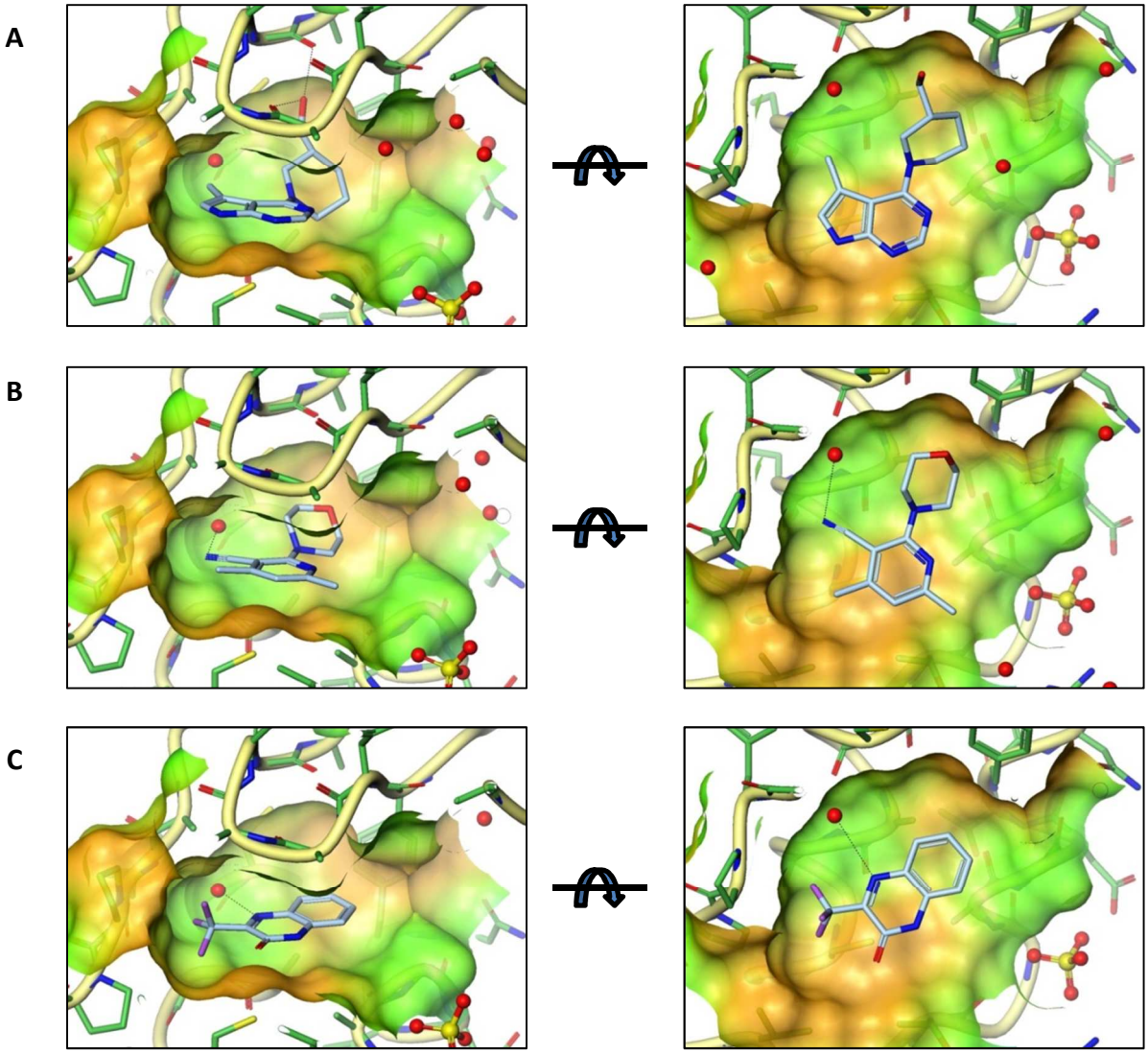


**Figure 3.** Binding modes of fragment hits **3**-**5**, illustrating the three key interactions in the binding site highlighted in Figure 1. (A) Compound **3** contains a saturated ring with a polar substitution in the ribose pocket, making a hydrogen bond with the backbone carbonyl oxygen of Gly229 (PBD ID: 5WBM). (B) The nitrile group of **4** interacts with a conserved molecule of water deep in the binding pocket (PBD ID: 5WBO). (C) The trifluoromethyl group of **5** makes favorable hydrophobic interactions with the proline wall (PBD ID: 5WBP). A sulfate ion (drawn as a ball-and-stick model) from the crystallization buffer is seen in all three structures to be bound at the site previously occupied by the γ phosphate group of AMP-PNP.

Due to the identification of multiple fragment hits with similar binding modes, the Pfizer screening library was searched for compounds possessing an aryl core densely functionalized with substituents that could satisfy all three key interactions described above and illustrated in Figure 3. This approach led to the identification of compounds **7** and **8** where an alcohol-substituted pyrrolidine or piperidine was positioned to fill the ribose pocket, a nitrile group forms a hydrogen bound with the conserved water molecule and a trifluoromethyl group interacts with the proline wall (Figure 4).

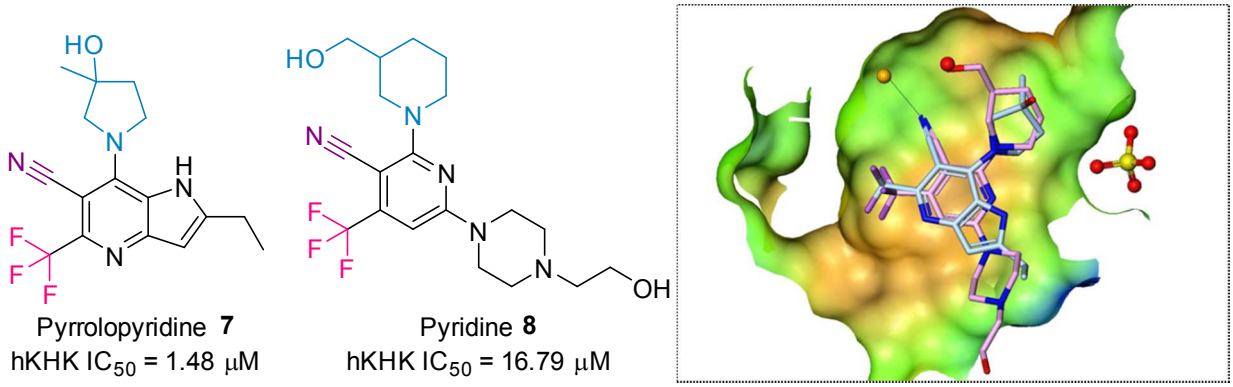


**Figure 4.** Compounds **7** (blue in the crystal structure, PBD ID: 5WBQ) and **8** (pink in the crystal structure, PBD ID: 5WBR) with improved potency against hKHK. The functional groups identified in blue, purple and pink reproduce the key interactions described for the fragments hits in Table 1 and Figure 3. In this figure, which shows the binding site in exactly the same view as the right hand panel of Figure 3, all protein atoms have been hidden for clarity. The nitrile group in both compounds interacts with a conserved water molecule, shown as a gold sphere. A second water molecule, shown as a red sphere, is seen in the crystal structure of **7**, which occupies the same space as that filled by the hydroxyl group in **8**.

As described in Table 2, pyrrolopyridine **7** is a hKHK inhibitor with moderate potency and low metabolic stability in human liver microsome (HLM) assays.[20] As observed in the crystal

structure (Figure 4), the ethyl substitution at the C2 position does not make any important interactions and was therefore removed without loss of potency. This modification significantly decreased LogD and resulted in much improved metabolic stability in the HLM assay (Table 2). The methylpyrrolidinol group was found to complement the ribose pocket with the *S* enantiomer **9** found to be more potent than the *R* enantiomer **10**.

**Table 2.** Structure-activity relationship (SAR) with the pyrrolopyridine core

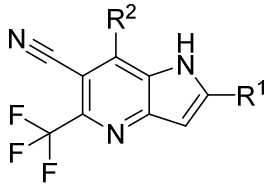


| Compound | $R^1$ | $R^2$ | hKHK $IC_{50}$ (μM)[a] ($pIC_{50}$±SD) | SFLogD[b] | HLM $Cl_{app}$[c] (μL/min/mg) |
|---|---|---|---|---|---|
| **7** | Et | 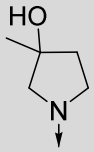 | 1.48 (5.8 ± 0.1) | 2.8 | 103 |
| **9** | H | 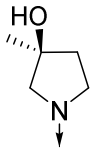 | 0.67 (6.17 ± 0.08) | 2.2 | <8 |
| **10** | H | 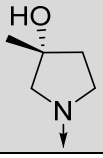 | 24.21 (4.62 ± 0.01) | 2.1 | <8 |

[a]$IC_{50}$ values for hKHK are reported as the mean of 3 replicates with $pIC_{50}$ ± SD in parentheses. [b]LogD values were determined using the shake-flask method with an octanol:water partition at pH 7.4.[21] [c]Apparent clearance from human liver microsomes.[20]

As depicted in Figure 5, pyrrolopyridine **9** was identified as a relatively potent and efficient human and rat KHK inhibitor with adequate microsomal stability, permeability ($P_{app}$)[22] and thermodynamic solubility. When evaluated in rat PK studies, a mean free $C_{max}$ of 1.3 μM with

high inter-animal variability was observed following oral administration at a high dose of 300 mg/kg. With an $IC_{50}$ of 0.64 μM against the rKHK, this exposure profile did not allow complete inhibition of KHK activity over a timeframe suitable for studying metabolic endpoints in vivo, thus further improvement of the series was pursued.

**A**

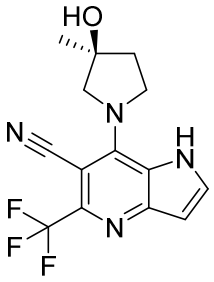


**9**

hKHK $IC_{50}$ = 0.67 μM[a]
rKHK $IC_{50}$ = 0.64 μM[a]
HLM $Cl_{app}$ <8 μL/min/mg
$P_{app}$ = 14 x$10^{-6}$ cm/s[b]
Therm. Sol. = 147 μM[c]
Fu = 0.032[d]

**B**

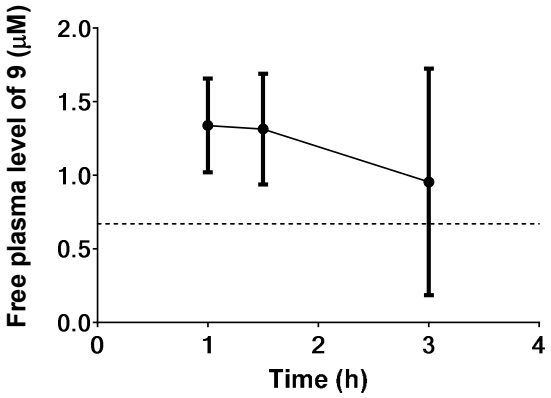


**Figure 5.** (A) In vitro profile of pyrrolopyridine **9**. [a]$IC_{50}$ values for hKHK and rKHK are reported as the mean of 3 replicates ($pIC_{50}$ = 6.17 ± 0.08 and 6.19 ± 0.01, respectively). [b]Permeability ($P_{app}$) was assessed in Ralph Russ canine kidney cells.[22] [c]Thermodynamic solubility was measured at pH 7.4. [d]Fu = faction unbound in plasma as assessed by equilibrium dialysis.[23] (B) Free plasma level of **9** in rat PK studies. 300 mg/kg dose was administered orally using 0.25% HPC-SL/0.05% DOSS as vehicle. Data presented as mean values (± standard deviation) with n = 3 per data point. Solid line = exposure. Dashed line = in vitro rKHK $IC_{50}$.

Since the substituents of pyrrolopyridine **9** recapitulated all three important interactions observed with the fragment hits (Figures 3 and 4), efforts to further improve the series were focused on the heteroaromatic core. When comparing the crystal structures of pyrrolopyridine **7** and pyridine **8**, the two scaffolds overlapped well and both displayed all three critical interactions with the ribose

pocket, conserved water molecule and hydrophobic pocket of KHK (Figure 4). Although pyridine **8** is a weaker KHK inhibitor, presumably due to suboptimal interaction of the functionalized piperidine ring in the ribose pocket, it offered an additional and synthetically enabled vector that was targeted for further optimization. As illustrated in Figure 6, merging functionalities from compounds **9** and **8** provided compound **11**, which displayed moderate KHK inhibitory potency (hKHK $IC_{50}$ = 1.03 μM) and microsomal stability (HLM $Cl_{app}$ = 14 μL/min/mg) in a reasonable LogD space (SFLogD = 2.2).

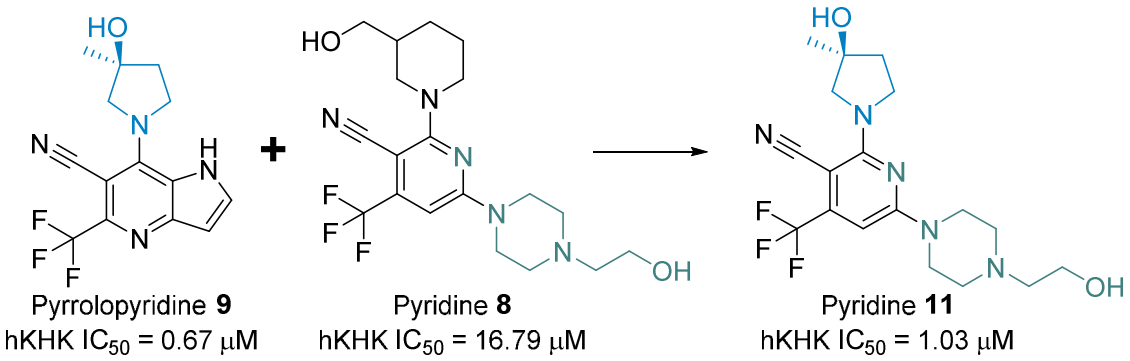


**Figure 6.** Merging pharmacophores led to the identification of pyridine **11**.

Using parallel chemistry, the piperazine vector of **11** was rapidly explored. In order to avoid discrepancies between potency against human and rat KHK (vide supra), neutral analogs were the key focus of optimization efforts. The optimal balance of potency, physical properties and clearance was achieved with trans-dihydroxy pyrrolidine analog **12** having a hKHK $IC_{50}$ value of 0.45 μM and no observable turnover in the HLM assay (Figure 7). The two hydroxyl groups form hydrogen bonds with solvent-exposed polar side chains Glu227 and Asn107, as well as with a bound water molecule. A complete map of interactions between compound **12** and hKHK is reported in Figure S3.

**A**

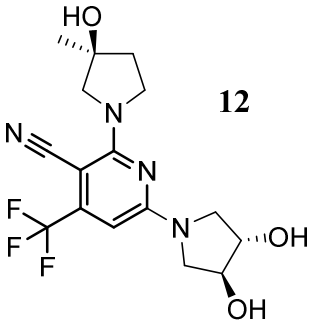


hKHK-C $IC_{50}$ = 0.45 µM[a]

hKHK-A $IC_{50}$ = 0.39 µM[b]

rKHK $IC_{50}$ = 0.34 µM[a]

SFLogD = 2.2

HLM $Cl_{app}$ <8 µL/min/mg

RLM $Cl_{app}$ <8 µL/min/mg

$P_{app}$ = 3.5 x$10^{-6}$ cm/s

Therm. $Sol._{7.4}$ = 503 µM

Fu = 0.13

**B**

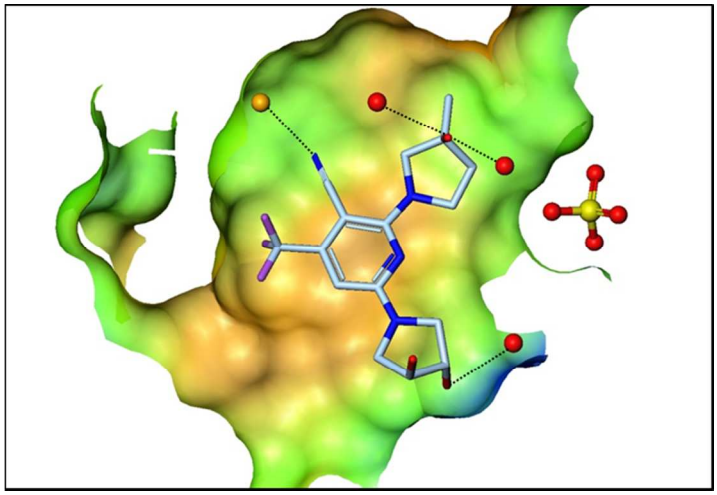

**C**

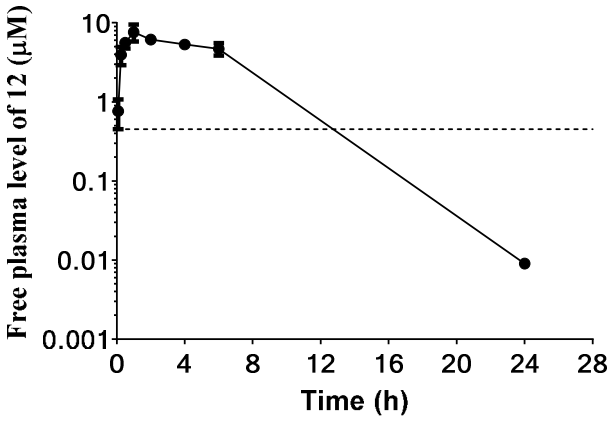


**Figure 7.** (A) Structure and profile of pyridine **12** in in vitro assays. [a]$IC_{50}$ values for rat and human KHK-C inhibition are reported as the mean of 19 replicates ($pIC_{50}$ = 6.3 ± 0.2 and 6.5 ± 0.2 respectively). [b]$IC_{50}$ value for hKHK-A inhibition is reported as the mean of four replicates ($pIC_{50}$ = 6.41 ± 0.09). RLM = rat liver microsomes. (B) The binding mode of **12** in the crystal structure (PBD ID: 5WBZ) is reported with a view of the binding site that is identical to the right panel of Figures 3 and 4. All protein atoms have been hidden for clarity. (C) Free plasma level of **12** in rat PK studies. A 150 mg/kg dose was administered orally using 1% polyvinylpyrrolidone / 0.025% sodium lauryl sulfate / 1% pluronic (nanocrystal suspension) as vehicle. Data presented

as mean values (± standard deviation) with n = 4 per data point. Solid line = exposure. Dashed line = in vitro rKHK $IC_{50}$.

Pyridine **12** does not interact directly with Asp27(B) and inhibited rKHK and both human isoforms with comparable potency in enzymatic assays. On the basis of its high metabolic stability in rat liver microsomes (RLM), improved solubility and acceptable permeability (Figure 7A), compound **12** progressed to PK studies in rats. As determined with a 1 mg/kg intravenous (i.v.) dose, **12** demonstrated moderate in vivo systemic clearance (25.9 mL/min/kg), moderate volume of distribution (1.38 L/kg) and short effective half-life (1.2 h) in rats. When orally dosed at 5 mg/kg using 0.5% methylcellulose as the vehicle, **12** exhibited an oral bioavailability of 45% ($C_{max}$ = 2.94 μg/mL, $AUC_{last}$ = 14.5 μg·h/mL) in rats. Free plasma concentration equivalent to multiples over the in vitro $IC_{50}$ were achieved for an extended period of time (~14 hours) at an oral dose of 150 mg/kg (Figure 7C).

Compound **12** showed high selectivity for KHK with no significant activity detected against a broad panel of transporters, receptors, ion channels and enzymes, including the hERG channel and major human CYP450s (Table S1). Overall, **12** had a clean in vitro safety profile with no genetic toxicology risks identified in Ames mutagenicity and in vitro micronucleus assays, and no toxicity was observed in HepG2 cells at concentrations up to 300 μM with 72 hour incubation. Supported by inhibitory potency against rKHK (Figure 7A), suitable exposure in rat PK studies (Figure 7B) and clean in vitro safety profile, compound **12** was resynthesized on larger scale to enable the evaluation of KHK inhibition in vivo.

Sprague Dawley rats were utilized to demonstrate KHK inhibition in vivo, focusing on the liver and kidney which are primary sites of KHK-C expression and fructose metabolism. All

procedures performed on these animals were in accordance with regulations and established guidelines and were reviewed and approved by the Pfizer Institutional Animal Care and Use Committee. Sprague Dawley rats were administered increasing oral doses of compound **12** followed by an i.v. bolus of fructose. Two minutes after fructose administration, animals were sacrificed and the liver and kidney tissues were removed and snap-frozen in liquid nitrogen. F1P was directly quantified in liver and kidney tissues by liquid chromatography/mass spectrometry (LC/MS). Direct F1P quantitation is challenging due to highly abundant sugar monophosphate isomers, such as glucose-6-phosphate (G6P), fructose-6-phosphate (F6P), and glucose-1-phosphate (G1P). Because the isomers have one common m/z, selectivity may not be achieved in the mass spectrometer; rather, they must be separated chromatographically. Widely adopted MS-compatible LC methods result in poor separation or co-elution of hexose monophosphate isomers. Therefore, an in-house ion exchange liquid chromatography method, which maintains compatibility with MS, was developed to address this problem. Using this method, dose-dependent decreases in both liver and kidney F1P concentrations were measured with $ED_{50}$ values of 30.0 mg/kg and 15.7 mg/kg, respectively (Figure 8). The decrease in both liver and kidney F1P levels indicates potent KHK inhibition in these tissues.

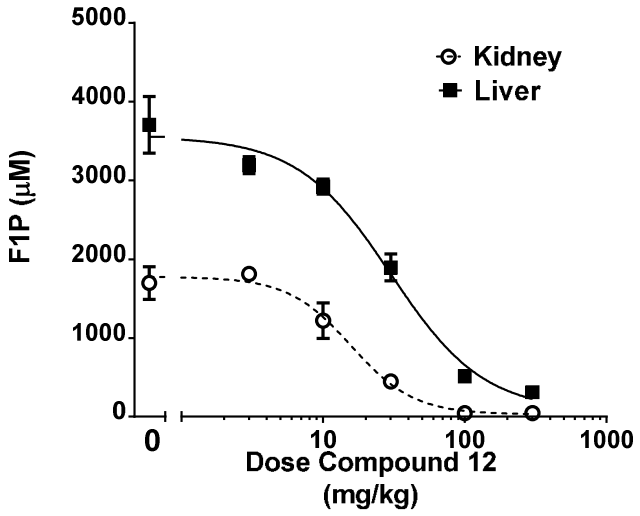


| | Kidney | Liver |
|---|---|---|
| $ED_{50}$ (mg/kg) | 15.7 | 30.0 |
| $pED_{50}$ ± SE | 1.20 ± 0.08 | 1.48 ± 0.09 |

**Figure 8.** Concentrations of hepatic and renal fructose-1-phosphate (F1P) following an i.v. bolus of fructose and increasing doses of compound **12** in Sprague Dawley rats. A non-linear dose response curve was fitted to a variable slope (four parameter) using GraphPad Prism and the calculated $ED_{50}$ for kidney and liver F1P reduction are reported. Data presented as mean values (± standard error) with n = 7-8 per data point.

To determine the effect of compound **12** on systemic fructose metabolism, plasma fructose levels were measured following an oral bolus of fructose. Sprague Dawley rats were treated with increasing doses of compound **12** and then administered a 2 g/kg oral bolus of fructose. Because KHK is the primary enzyme responsible for metabolic clearance of fructose, treatment with compound **12** was anticipated to increase plasma fructose levels. Indeed, a dose-dependent increase in plasma fructose levels was observed (Figure 9), suggesting that compound **12** inhibited systemic fructose metabolism. Taken together, these data support that oral

administration of compound **12** inhibits hepatic and renal fructose metabolism in rats, resulting in decreased formation of F1P in these organs and increased fructose concentration in plasma. Future studies will be informative as to the degree of KHK inhibition required for metabolic benefit since no clinical and non-clinical data has been reported with a KHK inhibitor.

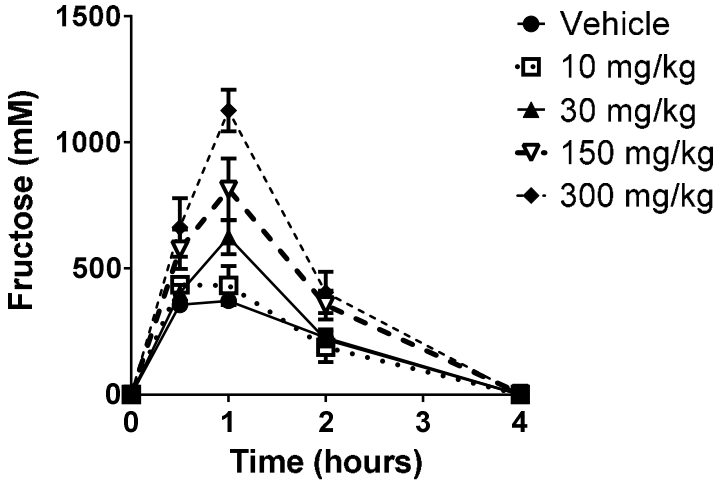


**Figure 9.** Plasma fructose levels in Sprague Dawley rats following an oral fructose bolus and treatment with the indicated dose of compound **12**. Animals were administered compound **12** orally one hour prior to an oral bolus of fructose (2 g/kg). Data presented as mean values (± standard error) with n = 6-8 per data point.

SYNTHESIS

The synthesis of the pyrrolopyridine series began with construction of pyrrole **15** (Scheme 1). Cyanogen bromide was first reacted with phenol and subsequent $S_N2$ displacement with 1-butyne led to nitrile **14**. Condensation with diethyl aminomalonate led to formation of pyrrole **15**. Pyrrole **16** was commercially available. Reaction of these aminopyrroles with tosylate **13** and

subsequent DBU-mediated ring closure led to pyrrolopyridine cores **17** and **18**. Chlorination and subsequent $S_NAr$ reactions led to the formation of **7**, **9**, and **10**.

**Scheme 1**. Synthesis of pyrrolopyridines **7**, **9**, and **10**

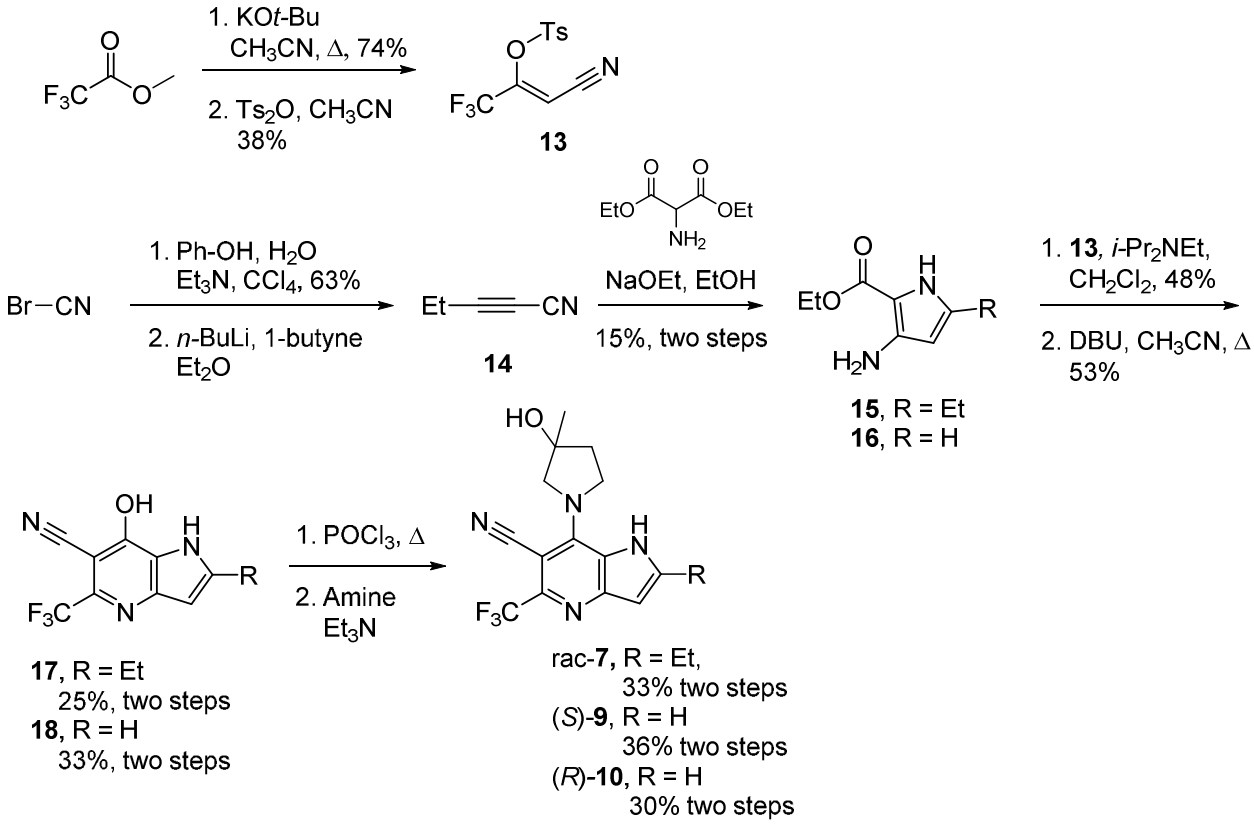


Pyridine **11** was constructed in a two-step $S_NAr$ sequence (Scheme 2). Starting from commercially available dichloropyridine **19**, amine addition at the 6-position occurred with good selectivity at ambient temperature to form pyridine **20**. Subsequent amine addition at the 2-position occurred at elevated temperatures to form pyridine **11**. Pyridine **8** was synthesized in an analogous manner.

**Scheme 2**. Synthesis of pyridine **11**

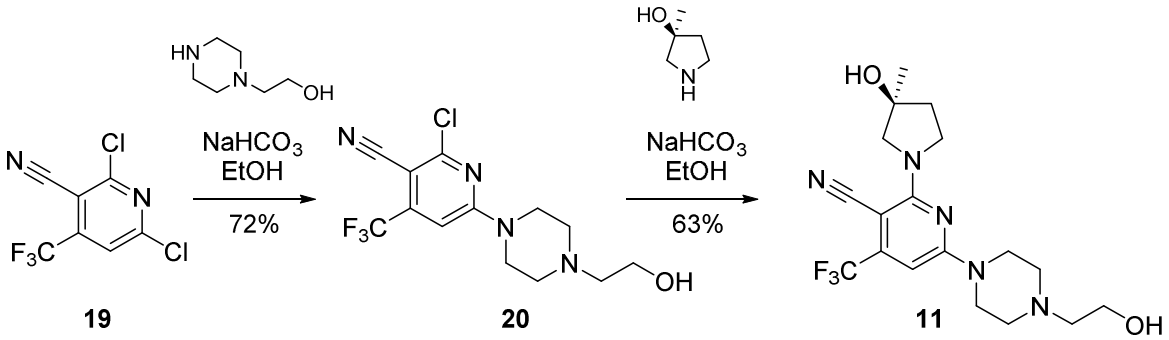


To provide sufficient quantities for the planned in vivo experiments, access to enantiopure **12** was required (Scheme 3). Addition of methyl magnesium bromide to *N*-benzyl-pyrrolidin-3-one (**21**) proceeded in good yield to provide the corresponding tertiary alcohol. Benzyl deprotection by hydrogenolysis led to alcohol **22**. Chiral resolution by preferential crystallization with L-dihydroorotic acid from ethanol followed by recrystallization from methanol produced the desired pure (*S*)-enantiomer. $S_NAr$ reaction of the core pyridine **19** with trans-dihydroxypyrrolidine **23** proceeded smoothly and isolation of the desired major regioisomer was achieved in good yield after crystallization. The final $S_NAr$ proceeded smoothly and 132 g of pyridine **12** was isolated by crystallization from MTBE in high yield.

**Scheme 3**. Synthesis of pyridine **12**

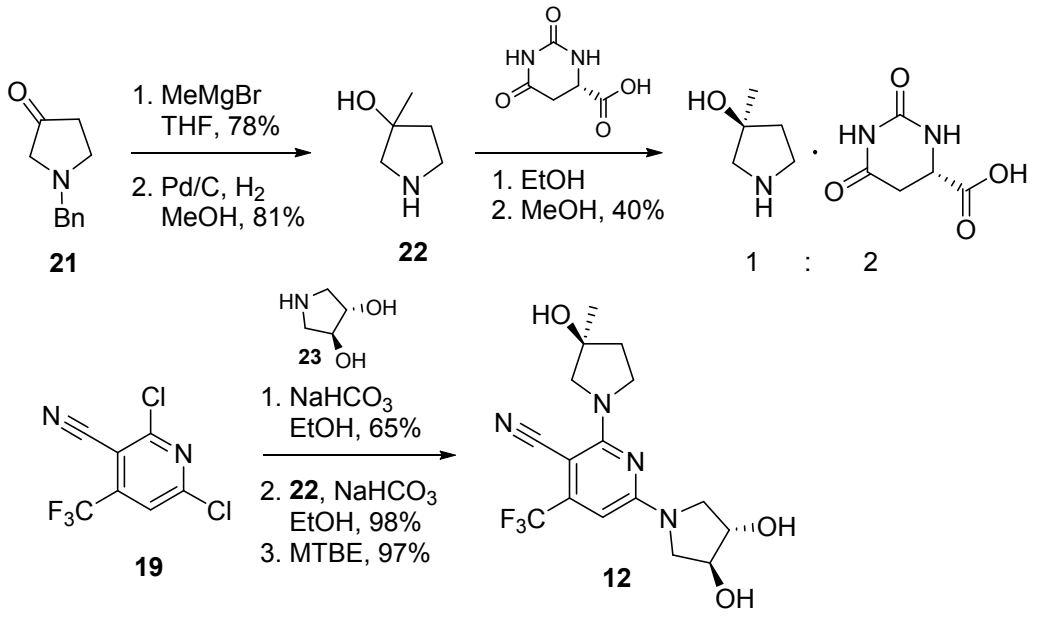


CONCLUSION

In this report we described the identification of fragments interacting with KHK which were subsequently optimized into moderately potent KHK inhibitors that could be used to modulate KHK activity in vivo. The fragment hits were identified via an NMR screen and confirmed by SPR. Selected fragments were co-crystallized with hKHK and a number of key interactions were observed with multiple fragments. In order to avoid discrepancy between the potencies against rat and human KHK, basic amines were avoided during optimization efforts. This led to the identification of pyridine **12**, a non-basic moderately potent and highly selective KHK inhibitor with favorable ADME and safety profiles and good exposure in rats. Compound **12** was synthesized on a scale needed to support in vivo experiments and inhibition of KHK and metabolism of fructose was demonstrated in rats. Compound **12** can facilitate the study of KHK as a potential therapeutic target.

EXPERIMENTAL SECTION

**General**. Unless otherwise noted, the reported experiments followed these general guidelines: All chemicals, reagents, and solvents were purchased from commercial sources when available and used without further purification**.** Compound **4** is commercially available from Enamine or previously reported in literature.[24] Compound **5** is commercially available from Enamine or previously reported in literature.[25] Compound **6** is previously reported in literature.[26] Air- and moisture-sensitive reactions were carried out under an inert atmosphere of nitrogen, magnetically stirred, and monitored by thin layer chromatography (TLC), high performance liquid chromatography (HPLC), or UPLC (ultra-performance liquid chromatography). Reactions were carried out at room temperature (~23 °C). Silica gel chromatography was performed using an automated system with pre-packaged columns. Concentration under reduced pressure (in vacuo) was performed by rotary evaporation at 25–45 °C. Purified compounds were further dried under high vacuum and/or heat to remove residual solvent. Yields refer to dried purified compounds. NMR spectra were recorded with either a spectrometer at 600 MHz or with a spectrometer at 400 MHz for $^{1}$H acquisitions. Chemical shifts were referenced to the residual $^{1}$H solvent signals ($CDCl_3$, δ 7.27; DMSO–$d_6$, δ 2.50; $CD_3OD$, δ 3.31). Signals are listed as follows: chemical shift in ppm; multiplicity identified as s = singlet, br = broad, d = doublet, t = triplet, m = multiplet; coupling constants in Hz. Liquid chromatography-mass spectrometry (LCMS) was performed via atmospheric pressure chemical ionization (AP) or electrospray ionization (ES) sources. Purity is reported by relative UV area and is >95% unless noted. Based on their structures, the compounds reported in this work are not predicted to be PAINS. Specific interaction with hKHK is supported by data from orthogonal assays (SPR, NMR, functional) and co-crystal structures

with hKHK. Additionally, compound **12** does not show activity in a number of assay formats as reported in the selectivity Table S1.

**Synthesis of analogues and intermediates**. *(R)-(1-(5-Methyl-7H-pyrrolo[2,3-d]pyrimidin-4-yl)piperidin-3-yl)methanol (**3**).* A vial was charged with 4-chloro-5-methyl-7H-pyrrolo[2,3-d]pyrimidine (100 mg, 0.60 mmol), (*R*)-piperidin-3-ylmethanol (82.5 mg, 0.72 mmol), Hünig's base (0.21 mL, 1.2 mmol), and acetonitrile (3 mL). The vial was sealed and heated to 60 °C for 15 h. The reaction was then cooled and poured onto half-saturated ammonium chloride and ethyl acetate. The layers were separated and organic layer was washed with saturated sodium bicarbonate solution, dried over sodium sulfate, filtered, and concentrated in vacuo. Flash column chromatography (20% ethyl acetate/heptane to 100% ethyl acetate to 10% methanol/ethyl acetate), taking the pure fraction to provide **3** (20 mg, 14%). LCMS (AP+) calc. for $C_{13}H_{18}N_4O$: 247.1; found: 247.3. $^1$H NMR (400 MHz, MeOH-$d_4$) δ 8.18 (s, 1H), 6.99 (d, *J*=1.2 Hz, 1H), 4.19–4.11 (m, 1H), 4.02–3.92 (m, 1H), 3.55 (dd, *J*=5.5, 10.9 Hz, 1H), 3.46 (dd, *J*=7.8, 11.3 Hz, 1H), 3.01 (ddd, *J*=2.7, 11.3, 12.8 Hz, 1H), 2.78 (dd, *J*=10.1, 12.9 Hz, 1H), 2.44 (d, *J*=1.2 Hz, 3H), 2.01–1.82 (m, 3H), 1.82–1.66 (m, 1H), 1.33–1.17 (m, 1H).

*2-Ethyl-7-(3-hydroxy-3-methylpyrrolidin-1-yl)-5-(trifluoromethyl)-1H-pyrrolo[3,2-b]pyridine-6-carbonitrile (**7**).* Step 1: A round bottomed flask was charged with **17** (25.0 g, 98.0 mol) and $POCl_3$ (40 mL) and the reaction was heated to reflux temperature for 2 h. The reaction was cooled to rt and the mixture was added dropwise to ice water. The mixture was then extracted with EtOAc (200 mL x 2) and the layers separated. The combined organic phases were washed with brine (150 mL), dried over $Na_2SO_4$ and concentrated in vacuo to give 7-chloro-2-ethyl-5-(trifluoromethyl)-1H-pyrrolo[3,2-b]pyridine-6-carbonitrile (19 g, 71%) as a grey solid. LCMS

(ES−) calc. for $C_{11}H_7ClF_3N_3$ (M−H): 272.0; found: 272.0. $^1$H NMR (400 MHz, $CDCl_3$) δ 9.10 (br. s, 1H), 6.73 (s, 1H), 2.97 (q, *J*=7.5 Hz, 2H), 1.45 (t, *J*=7.5 Hz, 3H).

Step 2: To a solution of 7-chloro-2-ethyl-5-(trifluoromethyl)-1H-pyrrolo[3,2-b]pyridine-6-carbonitrile (100 mg, 0.37 mol) and 3-methylpyrrolidin-3-ol (75 mg, 0.55 mmol) in DMF (2 mL) was added $Et_3N$ (110 mg, 1.09 mmol). The mixture was stirred for 16 hours at 80 °C. The mixture was purified by preparative TLC to give the **7** (72 mg, 59%) as a yellow solid. LCMS (ES+) calc. for $C_{16}H_{17}F_3N_4O$ (M+H): 339.1; found: 339.1. $^1$H NMR (400 MHz, $CD_3OD$) δ 6.43 (s, 1H), 4.52–4.42 (m, 1H), 4.16 (d, *J*=10.5 Hz, 1H), 4.13–4.05 (m, 1H), 3.86 (d, *J*=10.5 Hz, 1H), 2.87 (q, *J*=7.5 Hz, 2H), 2.19–1.96 (m, 2H), 1.53 (s, 3H), 1.35 (t, *J*=7.5 Hz, 3H).

*6-(4-(2-Hydroxyethyl)piperazin-1-yl)-2-(3-(hydroxymethyl)piperidin-1-yl)-4-(trifluoromethyl)nicotinonitrile (**8**).* A vial was charged with **20** (73 mg, 0.22 mmol), DMF (0.25 mL), piperidin-3-ylmethanol (25 mg, 0.22 mmol), and $K_2CO_3$ (35 mg, 0.25 mmol), and stirred at 100 °C for 2 h. The reaction was cooled to rt and diluted with ethyl acetate (3 mL) and half-saturated NaCl solution (3 mL). The layers were separated and the organic was concentrated in vacuo and purified via preparatory reverse-phase HPLC to provide **8** (48 mg, 53%). LCMS (ES+) calc. for $C_{19}H_{26}F_3N_5O_2$ (M+H): 413.2; found: 414.2. $^1$H NMR (400 MHz, MeOD-$d_4$) δ 6.54 (s, 1H), 4.34–4.27 (m, 1H), 4.24–4.13 (m, 1H), 3.79–3.74 (m, 4H), 3.72 (t, *J*=5.9 Hz, 2H), 3.55–3.39 (m, 2H), 3.06 (ddd, *J*=3.1, 11.7, 13.0 Hz, 1H), 2.82 (dd, *J*=9.4, 12.9 Hz, 1H), 2.64–2.60 (m, 4H), 2.59 (t, *J*=5.9 Hz, 2H), 1.93–1.74 (m, 3H), 1.74–1.57 (m, 1H), 1.36–1.22 (m, 1H).

*(S)-7-(3-Hydroxy-3-methylpyrrolidin-1-yl)-5-(trifluoromethyl)-1H-pyrrolo[3,2-b]pyridine-6-carbonitrile (**9**) and (R)-7-(3-hydroxy-3-methylpyrrolidin-1-yl)-5-(trifluoromethyl)-1H-pyrrolo[3,2-b]pyridine-6-carbonitrile (**10**).* Step 1: Compound **18** (200 g, 0.88 mol) was

dissolved in $CH_3CN$ (1.5 L). Then $POCl_3$ (673 g, 4.4 mol) was added carefully. After the addition, the resulting mixture was heated to 60 °C overnight. The reaction mixture was then cooled to rt and concentrated in vacuo. The residue was dissolved in ethyl acetate and slowly poured onto water (1.0 L). The layers were separated and the organic layer was washed with 10% $K_2CO_3$, dried over $Na_2SO_4$, filtered, and concentrated in vacuo. Flash column chromatography was then used to provide 7-chloro-5-(trifluoromethyl)-1H-pyrrolo[3,2-b]pyridine-6-carbonitrile (105 g, 49%). LCMS calc. for $C_9H_3ClF_3N_3$ (M+H): 246.0; found: 245.7 (M+H). $^1$H NMR (400 MHz, DMSO-$d_6$) δ 13.11 (br. s, 1H), 8.29 (t, *J*=2.8 Hz, 1H), 7.04 (dd, *J*=3.0, 2.0 Hz, 1H).

Step 2 (milligram synthesis): To a solution of 7-chloro-5-(trifluoromethyl)-1H-pyrrolo[3,2-b]pyridine-6-carbonitrile (400 mg, 1.64 mmol) and 3-methylpyrrolidin-3-ol (320 mg, 2.34 mmol) in DMF (5 mL) was added $Et_3N$ (500 mg, 4.95 mmol). The mixture was then stirred at 80 °C for 2 h. The mixture was then poured onto water (40 mL) and extracted with EtOAc (40 mL x 3). The organic layer was washed with $H_2O$ (30 mL x 3), brine (30 mL x 3), dried over $Na_2SO_4$, filtered, and concentrated in vacuo. The material was then purified by flash chromatography (0% to 70% EtOAc/petroleum ether to provide clean racemic material (360 mg, 71%) as yellow solid. The enantiomers were then separated by chiral SFC (column: Chiralpak IC-3 150×4.6 mm I.D., 3 um; mobile phase: ethanol (0.05% DEA) in $CO_2$ from 5% to 40%; flow rate: 2.35 mL/min) to provide the two separated enantiomers:

**9**: 150 mg, retention time: 4.123; LCMS (ES+) calc. for $C_{14}H_{13}F_3N_4O$ (M+H): 311.1; found: 310.9. $^1$H NMR (400 MHz, MeOD) δ 7.54 (d, *J*=3.0 Hz, 1H), 6.62 (d, *J*=3.0 Hz, 1H), 4.48–4.38 (m, 1H), 4.16–4.03 (m, 2H), 3.90–3.81 (m, 1H), 2.12–1.97 (m, 2H), 1.49 (s, 3H). $[\alpha]^{20}_D$ +19.2 (c 0.64, $CH_3OH$).**10**: 160 mg; er: 98.9:1.1; retention time: 4.414; LCMS (ES+) calc. for

$C_{14}H_{13}F_3N_4O$ (M+H): 311.1; found: 310.9. $^1$H NMR (400 MHz, MeOD) δ 7.54 (d, *J*=3.0 Hz, 1H), 6.62 (d, *J*=3.0 Hz, 1H), 4.48–4.38 (m, 1H), 4.16–4.03 (m, 2H), 3.90–3.81 (m, 1H), 2.12–1.97 (m, 2H), 1.49 (s, 3H). $[\alpha]^{20}_D$ –22.2 (c 1.00, $CH_3OH$).

*(S)-7-(3-Hydroxy-3-methylpyrrolidin-1-yl)-5-(trifluoromethyl)-1H-pyrrolo[3,2-b]pyridine-6-carbonitrile (**9**, multi-gram synthesis)*

Step 1: A three-neck flask equipped with an addition funnel and thermometer was charged with methyl magnesium bromide (3.0 M in ether, 30 mL, 90 mmol) and tetrahydrofuran (100 mL) and cooled to -78 °C. A solution of benzyl 3-oxopyrrolidine-1-carboxylate (9.80 g, 44.7 mmol) in tetrahydrofuran (100 mL) was then added dropwise, keeping the internal temperature < -70 °C. The reaction was then warmed to rt for 1 h then cooled to 0 °C and quenched with saturated ammonium chloride (150 mL) with a slight exotherm. The mixture was then extracted with MTBE (3 x 100 mL). The combined organic layers were dried over magnesium sulfate, filtered, and concentrated in vacuo. The crude product was purified by flash column chromatography (0–100% ethyl acetate/heptane) to provide crude racemic product. Chiral SFC was then used to isolate benzyl (*S*)-3-hydroxy-3-methylpyrrolidine-1-carboxylate (3.0 g, 29%) as peak 1 (column: Chiral Tech ID 250 mm x 21.2 mm 5 um; isocratic, 90% $CO_2$, 9.8% MeOH, 0.2% $NH_4OH$, detection: 210 nm; flow rate: 80.0 mL/min; backpressure: 120 Bar). LCMS (AP+) calc. for $C_{13}H_{17}NO_3$ (M+H): 236.1; found: 236.0. $^1$H NMR (400 MHz, $CDCl_3$) δ 7.45–7.25 (m, 5H), 5.25–5.03 (m, 2H), 3.67–3.43 (m, 3H), 3.38–3.22 (m, 1H), 2.00–1.73 (m, 3H), 1.42 (s, 3H).

Step 2: A Parr reactor was charged with benzyl (*S*)-3-hydroxy-3-methylpyrrolidine-1-carboxylate (3.50 g mg, 14.9 mmol), Pd/C (wet, 10 wt%, 792 mg, 0.025 mmol) and ethanol (50 mL) then charged with 30 psi hydrogen and stirred for 5 h (recharging $H_2$ pressure after 2 h). The

reactor was vented and purged with nitrogen. The mixture was filtered through celite, rinsing with ethanol. The filtrate was then concentrated in vacuo to provide (*S*)-3-methylpyrrolidin-3-ol (1.51 g, *quant.*) as an oil that was taken into the next step without further purification.

Step 3: A round bottomed flask was charged with (*S*)-3-methylpyrrolidin-3-ol (1.41 g, 13.9 mmol), 7-chloro-5-(trifluoromethyl)-1H-pyrrolo[3,2-b]pyridine-6-carbonitrile (2.85 g, 11.6 mmol) and acetonitrile (40 mL). Triethyl amine (3.26 mL, 23.3 mmol) was then added and the reaction heated to 80 °C for 1.5 h. Additional (*S*)-3-methylpyrrolidin-3-ol (270 mg, 2.67 mmol) was then added and the reaction stirred at 80 °C for 20 minutes. The reaction was cooled to rt and diluted with saturated ammonium chloride and ethyl acetate. The layers were separated and the aqueous layer was extracted with ethyl acetate (x 3). The combined organic layers were washed with saturated sodium bicarbonate solution, then brine, and dried over sodium sulfate, filtered, and concentrated in vacuo. Ethanol (80 mL) was added to the resultant residue and the mixture was heated to reflux then cooled to rt. Solids formed that were collected via filtration and washed with ethanol to provide crude product (1.55 g, 43%). Several batches of material were combined (4.05 g) and diluted with acetonitrile (120 mL) then heated to reflux then cooled to rt over 45 minutes while stirring. The resultant solids were filtered, washed with acetonitrile, and dried in vacuo. The solids were then added to methanol and heated to dissolve. The mixture was concentrated in vacuo to provide the desired crystalline product (3.145 g, 78%) er: >99.95:0.05 (determined by chiral SFC). LCMS (ES+) calc. for $C_{14}H_{13}F_3N_4O$ (M+H): 311.1; found: 311.2. $^1$H NMR (400 MHz, DMSO) δ 11.64 (br. s, 1H), 7.68 (d, *J*=3.1 Hz, 1H), 6.67 (d, *J*=3.1 Hz, 1H), 5.03 (br. s, 1H), 4.41–4.24 (m, 1H), 4.15–3.92 (m, 2H), 3.77 (d, *J*=10.5 Hz, 1H), 1.96 (s, 2H), 1.41 (s, 3H). m.p. 264.2–264.3 °C.

*(S)-2-(3-Hydroxy-3-methylpyrrolidin-1-yl)-6-(4-(2-hydroxyethyl)piperazin-1-yl)-4-(trifluoromethyl)nicotinonitrile (**11**).* To a mixture of **20** (60 mg, 0.18 mmol) and (*S*)-**22** (60 mg, 0.19 mmol) in DMF (2 mL) was added $Et_3N$ (0.2 mL), then the mixture was stirred at 60 °C for 20 h. The reaction was filtered and the filtrate was concentrated and purified by preparatory reverse-phase HPLC to provide **11** (38 mg, 63%) as a white solid. LCMS (ES+) for $C_{18}H_{24}F_3N_5O_2$ (M+H): 400.2; found: 400.0. $^1$H NMR (400 MHz, MeOH-$d_4$) δ 6.45 (s, 1H), 4.04–3.63 (m, 10H), 2.72–2.59 (m, 6H), 2.03–1.91 (m, 2H), 1.44 (s, 3H).

*6-((3S,4S)-3,4-Dihydroxypyrrolidin-1-yl)-2-((S)-3-hydroxy-3-methylpyrrolidin-1-yl)-4-(trifluoromethyl)nicotinonitrile (**12**).* Step 1: A round bottomed flask was charged with 2,6-dichloro-4-(trifluoromethyl)nicotinonitrile (66.8 g, 647 mmol), sodium bicarbonate (105 g, 1.25 mol), and ethanol (1.56 L). (3S,4S)-pyrrolidine-3,4-diol (150.0 g, 622.4 mmol) was then added in portions over 40 minutes while maintaining the internal temperature < 4 °C. The reaction was then warmed to rt and stirred for 22 h. The reaction was cooled to 0 °C and additional sodium bicarbonate (77.0 g, 917 mmol) that was ground in a mortar and pestle was added in one portion and the mixture stirred for 22 h at rt. The solids were filtered and the filtrate concentrated to a slurry (~1/4 of the original volume). Water (100 mL) was added and the mixture was stirred at rt for 1 h. The solids were collected via filtration, washed with water then dried in a vacuum oven at 50 °C to provide crude material (186.0 g). This material was split into two equal portions (93.0 g x 2) and each was dissolved in ethyl acetate (830 mL) in a round bottomed flask at reflux temperature. Heptane (2.1 L) was then added to each batch and the mixture was slowly cooled to rt over 4 h then stirred for an additional 15 h at rt. The solids were collected via filtration and combined to provide 148.0 g. The solids were then added to MTBE (1.5 L) in a round bottomed flask and heated to 56 °C. Heptane (1.0 L) was then added via addition funnel over 30 minutes

and the mixture was cooled to rt and the solids were collected via filtration, washed with MTBE-heptane (3:2) and dried in a vacuum oven at 40 °C to obtain 2-chloro-6-((3*S*,4*S*)-3,4-dihydroxypyrrolidin-1-yl)-4-(trifluoromethyl)nicotinonitrile (123.87 g, 65%). LCMS (ES+) calc. for $C_{11}H_9ClF_3N_3O_2$ : 308.0; found: 308.0. $^1$H NMR (600 MHz, DMSO-$d_6$) δ 6.94 (s, 1H), 5.36 (d, *J*=3.5 Hz, 1H), 5.28 (d, *J*=3.5 Hz, 1H), 4.11 (br. s, 1H), 4.06 (br. s, 1H), 3.71 (dd, *J*=3.5, 11.7 Hz, 1H), 3.64 (dd, *J*=2.9, 12.9 Hz, 1H), 3.57 (d, *J*=11.2 Hz, 1H), 3.46 (d, *J*=11.7 Hz, 1H).

Step 2: A round bottomed flask was charged with 2-chloro-6-((3*S*,4*S*)-3,4-dihydroxypyrrolidin-1-yl)-4-(trifluoromethyl)nicotinonitrile (110.0 g, 357.5 mmol), (*S*)-3-methylpyrrolidin-3-ol/L-dihydroorotic acid complex (1:2, 160.0 g, 383.3 mmol), sodium bicarbonate (120.0 g, 1430 mmol), and ethanol (1.1 L) then the mixture was heated to 77 °C (internal temperature) for 24 h with overhead stirring. Additional sodium bicarbonate (80.0 g, 952 mmol) was ground in a mortar and pestle then added to the reaction, which was stirred at 77 °C for an additional 24 h. The mixture was cooled to room temperature and filtered. The filtrate was partially concentrated in vacuo at 50 °C until a light slurry formed (~1/4 of the initial volume). The slurry was stirred at rt and slowly water (1.0 L) was added. The mixture was stirred at rt for 18 h, then the solid was filtered off, washed with water, and dried in vacuo at 60 °C for 18 h to obtain the title compound (129.9 g, 98%). This material was combined with two smaller batches (4.9 g and 1.5 g) and stirred in MTBE (2.0 L) at 50 °C for 20 h, then rt for 3 h. The solids were collected via filtration, washed with MTBE, and dried in vacuo at 60 °C for 20 h to obtain crystalline **12** (131.9 g, 97%). HPLC: 99.54%. LCMS (ES+) calc. for $C_{16}H_{19}F_3N_4O_3$ (M+H): 373.1; found: 373.1. $^1$H NMR (400 MHz, DMSO-$d_6$) δ 6.18 (s, 1H), 5.23 (d, *J*=3.5 Hz, 1H), 5.16 (d, *J*=3.1 Hz, 1H), 4.83 (s, 1H), 4.10–4.04 (m, 1H), 4.04–3.97 (m, 1H), 3.82 (dt, *J*=7.4, 10.1 Hz, 1H), 3.72 (ddd, *J*=2.9, 7.9,

10.6 Hz, 1H), 3.66–3.48 (m, 5H), 3.36–3.28 (m, 1H), 1.95–1.78 (m, 2H), 1.33 (s, 3H). m.p. 202–204 °C. $[\alpha]^{20}_{D}$ +3.5 (c 0.51, $CH_3OH$).

*1-Cyano-3,3,3-trifluoroprop-1-en-2-yl 4-methylbenzenesulfonate (**13**).* Step 1: To a suspension of potassium tert-butoxide (706 g, 6.30 mol) in toluene (8.0 L) was added dropwise a solution of methyl trifluoroacetate (895 g, 6.30 mol) in $CH_3CN$ (258 g , 6.30 mol), at which time internal temperature was increased to 70 °C. After the addition, the resulting mixture was heated to 80 °C for 4 hours, the reaction mixture was cooled to room temperature and filtered to give potassium (*Z*)-1-cyano-3,3,3-trifluoroprop-1-en-2-olate (820 g, 74%) as yellow solid. $^1$H NMR (400 MHz, $D_2O$) δ 4.56 (s, 1H).

Step 2: To a suspension of potassium (*Z*)-1-cyano-3,3,3-trifluoroprop-1-en-2-olate (980 g, 5.6 mol) in MeCN (15 L) was added *p*-toluenesulfonic anhydride (1460 g, 4.48 mol) in portions at rt. After the addition was complete, the reaction mixture was refluxed under intense stirring for 20 h. The reaction mixture was cooled and evaporated to remove most of the solvent and the residue was portioned between EtOAc (10 L) and water (8 L), further extracted with EtOAc (10 L), the combined organic extracts were washed with water (15 L) and brine (15 L), dried over $Na_2SO_4$ and concentrated to dryness, which was purified by column chromatography to give **13** (440 g, 38%) as yellow oil (4:1 mixture of geometrical isomers). $^1$H NMR (400 MHz, $CDCl_3$) *major*: δ 7.97 (d, *J*=8.5 Hz, 2H), 7.47–7.42 (m, 2H), 6.02 (s, 1H), 2.51 (s, 3H). *minor*: δ 7.85 (d, *J*=9.0 Hz, 2H), 7.44 (d, *J*=8.5 Hz, 2H), 6.15 (s, 1 H), 2.52 (s, 3H).

*Pent-2-ynenitrile (**14**).*Step 1: A round bottomed flask was charged with cyanogen bromide (250 g, 2.66 mol) and water (500 mL) and the suspension was cooled in an ice water bath. A solution of phenol (293 g, 2.79 mol) in $CCl_4$ (800 mL) was then added to the mixture in one portion,

followed by the addition of $Et_3N$ (385 mL) at a rate to keep the internal temperature below 5 °C. After the addition, the mixture was stirred at this temperature for 4 h. The layers were separated and the organic layer was washed with water (500 mL × 3), then dried over $Na_2SO_4$, filtered and concentrated in vacuo provide cyanatobenzene (200 g, 63%) as a brown oil, which was used directly in the next step without further purification.

Step 2: A round bottomed flask was charged with butyne (60 g, 1.1 mol) and ether (1.2 L) then cooled to −60 °C under nitrogen. *n*-BuLi in hexane (444 mL, 1.10 mol) was then added dropwise, followed by the addition of a solution of cyanatobenzene (131 g, 1.1 mol) in ether (300 mL), keeping the temperature < −60 °C. The mixture was stirred at −60 °C for 2 h then warmed to rt. The reaction was quenched with the addition of 6 N aq. NaOH (100 mL) and the layers separated. The aqueous phase was extracted with ether (300 mL × 3). The combined organic phases were washed with 6 N aq. NaOH (100 mL × 3), dried over $Na_2SO_4$, filtered, and used directly in the next step as a solution of **14** in ether.

*Ethyl 3-amino-5-ethyl-1H-pyrrole-2-carboxylate (**15**).* A round bottomed flask was charged with anhydrous EtOH (700 mL). Sodium (51 g, 2.2 mol) was then added in portions. After dissolution had occurred, diethyl 2-aminomalonate hydrochloride (234 g, 1.11 mol) was added and the mixture was stirred for 30 min. A solution of **14** (88 g, 1.11 mol in ether) was then added and the reaction was stirred at rt for 4 h. The mixture was then concentrated in vacuo and the resultant residue was diluted with water (250 mL) and extracted with ethyl acetate (5000 mL × 3). The organic layer was dried over $Na_2SO_4$, filtered, and concentrated in vacuo to give a crude product, which was further purified via flash column chromatography (ethyl acetate: petroleum ether = 1:50) to give **15** (30 g, 15%) as a yellow oil. LCMS (ES+) calc. for $C_9H_{14}N_2O_2$ (M+H): 183.1;

found: 183.1. $^1$H NMR (400 MHz, $CDCl_3$) δ 8.51–7.52 (br. m, 1H), 5.49 (d, *J*=2.5 Hz, 1H), 4.43–4.03 (br. m, 4H), 2.54 (q, *J*=7.5 Hz, 2H), 1.35 (t, *J*=7.0 Hz, 3H), 1.22 (t, *J*=7.5 Hz, 3H).

*2-Ethyl-7-hydroxy-5-(trifluoromethyl)-1H-pyrrolo[3,2-b]pyridine-6-carbonitrile (**17**).* Step 1: A round bottomed flask was charged with **15** (45.0 g, 0.249 mol), **13** (145 g, 0.498 mol), and $CH_2Cl_2$ (1.2 L) then cooled to 10 °C. Hünig's base (64.3 g, 0.498 mol) was added then the mixture warmed to rt and stirred overnight. The mixture was washed with water (100 mL × 3) and the organic layer was dried over $Na_2SO_4$, filtered, and concentrated in vacuo to provide a brown oil. Flash column chromatography (ethyl acetate/petroleum ether = 1:20) then provided ethyl 3-((1-cyano-3,3,3-trifluoroprop-1-en-2-yl)amino)-5-ethyl-1H-pyrrole-2-carboxylate (36 g, 48%) as a yellow solid that was taken forward without further purification.

Step 2: A round bottomed flask was charged with ethyl 3-((1-cyano-3,3,3-trifluoroprop-1-en-2-yl)amino)-5-ethyl-1H-pyrrole-2-carboxylate (30 g, 0.1 mol), DBU (15.2 g, 0.1 mol), and acetonitrile (300 mL) then heated to reflux temperature overnight. The reaction mixture was cooled to rt, and the solvents removed in vacuo to give a black solid. Flash column chromatography (ethyl acetate/petroleum ether = 1:5, then dichloromethane/methanol = 5:1) was used to provide **17** (20 g, 53%) as a yellow solid that was taken on to the next step.

*7-Hydroxy-5-(trifluoromethyl)-1H-pyrrolo[3,2-b]pyridine-6-carbonitrile (**18**).*Step 1: A round bottomed flask was charged with ethyl 3-amino-1H-pyrrole-2-carboxylate[27] (94.6 g, 0.614 mol) and $CH_3CN$ (1.5 L). **13** (187 g, 0.645 mol) and Hünig's base (119.73 g, 0.921 mol) were then added. The reaction mixture was heated to reflux for 6 h then cooled to rt. The material was concentrated in vacuo and purified by flash column chromatography (DCM:MeOH = 100:1) to provide ethyl 3-((1-cyano-3,3,3-trifluoroprop-1-en-2-yl)amino)-1H-pyrrole-2-carboxylate (94.5

g, 56.4%) as a yellow solid as a ~5:4 mixture of E/Z isomers. $^1$H NMR (400 MHz, DMSO-$d_6$) *major:* δ 9.07 (br. s, 1H), 7.07 (t, *J*=2.8 Hz, 1H), 6.32 (s, 1H), 4.89 (s, 1H), 4.24 (q, *J*=7.0 Hz, 2H), 1.27 (t, *J* =7.0 Hz, 3H). *minor:* δ 9.17 (br. s, 1H), 6.96 (t, *J*=3.0 Hz, 1H), 6.13 (t, *J*=2.8 Hz, 1H), 4.75 (s, 1H), 4.20 (q, *J*=7.0 Hz, 2H), 1.23 (t, *J* =7.0 Hz, 3H).

Step 2: A round bottomed flask was charged with ethyl 3-((1-cyano-3,3,3-trifluoroprop-1-en-2-yl)amino)-1H-pyrrole-2-carboxylate (204 g, 0.747 mol) and $CH_3CN$ (1.5 L). DBU (137.2 g, 0.897 mol) was then added and the reaction was heated to reflux for 12 h. The reaction was cooled to rt and concentrated in vacuo. Flash column chromatography was then used to provide **18** (100 g, 59%) as a yellow solid. $^1$H NMR (400 MHz, DMSO-$d_6$) δ 11.60 (br. s, 1H), 7.46 (t, *J*=3.0 Hz, 1H), 6.47 (dd, *J*=3.0, 2.0 Hz, 1H).

*2-Chloro-6-(4-(2-hydroxyethyl)piperazin-1-yl)-4-(trifluoromethyl)nicotinonitrile (**20**).* To a solution of 2,6-dichloro-4-(trifluoromethyl)nicotinonitrile (60 mg, 0.25 mmol) and 2-(piperazin-1-yl)ethan-1-ol (32 mg, 0.25 mmol) in DMF (2 mL) was added $NaHCO_3$ (42 mg, 0.50 mmol). Then the mixture was stirred at rt for 20 h. The mixture was quenched with brine (10 mL) and extracted with EtOAc (15 mL x 3). The combined organic layers were washed with $NH_4Cl$ (15 mL x 2), brine (15 mL x 2), dried over $Na_2SO_4$ and concentrated to give a residue which was purified by Prep-TLC ($CH_2Cl_2$:MeOH=20:1) to provide **20** (60 mg, 72 %) as a white solid. $^1$H NMR (400 MHz, MeOH-$d_4$) δ 7.12 (s, 1H), 3.84 (br. s, 4H), 3.72 (t, *J*=5.8 Hz, 2H), 2.71–2.65 (m, 4H), 2.62 (t, *J*=5.8 Hz, 2H).

*3-Methylpyrrolidin-3-ol (**22**).*Step 1: A solution of 1-benzylpyrrolidin-3-one (350 g, 2.0 mol) in THF (500 mL) was added dropwise to a stirred solution of MeMgBr (3.0 M, 1.0 L, 3.0 mol) in THF (2.0 L) at 0 °C. The reaction mixture was stirred at 0 °C for 1 h. The reaction mixture was

quenched with aqueous saturated $NH_4Cl$ (6.0 L) and the compound was extracted with ethyl acetate (1 L x 3). The organic layer was washed with brine, dried over sodium sulfate and concentrated in vacuo. The residue was purified on silica gel by flash chromatography (PE: EtOAc=5:1 to 1:1) to afford 1-benzyl-3-methylpyrrolidin-3-ol (300 g, 52%) as an oil. $^1$H NMR (400 MHz, $CDCl_3$) δ 7.36–7.20 (m, 5H), 3.64 (s, 2H), 3.03–2.90 (m, 1H), 2.73 (d, *J*=9.4 Hz, 1H), 2.38–2.28 (m, 1H), 2.23 (d, *J*=9.6 Hz, 1H), 1.95–1.84 (m, 2H), 1.35 (s, 3H)

Step 2: A suspension of 1-benzyl-3-methylpyrrolidin-3-ol (700 g, 3.66 mol) and 10% Pd/C (50% wet, 100 g) in MeOH (5.0 L) was placed under $H_2$ in a Parr bottle at 60 psi for 48 h. The reaction mixture was filtered through a short pad of celite and washed with MeOH. The filtrate was concentrated in vacuo to give **22** as an orange oil (300 g, 81%). $^1$H NMR (400 MHz, $CDCl_3$) δ 3.26–3.15 (m, 1H), 3.05–2.89 (m, 2H), 2.68 (d, *J*=11.5 Hz, 1H), 1.91–1.81 (m, 1H), 1.80–1.69 (m, 1H), 1.37 (s, 3H).

*(S)-3-Methylpyrrolidin-3-ol/L-dihydroorotic acid complex (1:2).* (*S*)-2,6-dioxohexahydropyrimidine-4-carboxylic acid (281 g, 1.78 mol) in ethanol (12 L) was heated to reflux then 3-methylpyrrolidin-3-ol (120 g, 1.19 mol) in ethanol (500 mL) was added dropwise at 85 °C for 1 h. The reaction was refluxed for 12 h, then cooled to rt overnight. The solids were collected via filtration, washed with ethanol (1.0 L), and dried in vacuo to afford the title compound (240 g). The product was re-crystallized by methanol (15 L x 4) to afford the title compound (60 g). The filtrates were concentrated and recrystallized by methanol (15 L) to afford a second crop of the product (40 g) for a total isolated amount of 100 g (20%). $^1$H NMR (400 MHz, DMSO-$d_6$) δ 10.09–9.46 (m, 3H), 7.42 (s, 2H), 3.94–3.77 (m, 2H), 3.31–3.15 (m, 2H), 2.99 (d, *J*=11.5 Hz, 1H), 2.90 (d, *J*=11.5 Hz, 1H), 2.74 (d, *J*=7.0 Hz, 1H), 2.70 (d, *J*=7.0 Hz, 1H),

2.54 (d, *J*=4.3 Hz, 1H), 2.51–2.45 (m, 1H), 1.90–1.69 (m, 2H), 1.30 (s, 3H).*ee% was checked by derivatization to Cbz-protected (S)-**22** and determined by SFC: >98% ee

**Protein expression and purification.** KHK protein sequences were obtained from NCBI under RefSeq ID's NP_006479.1 (human) and NP_114061.1 (rat). Plasmids were generated using pET28a(+) vector with N-terminal His-tag followed by thrombin cleavage sequence. Recombinant proteins were expressed in *E. coli* BL21 (DE3) following standard IPTG induction conditions, and purification of soluble protein was done using Ni-NTA affinity chromatography, followed by size exclusion chromatography and dialysis in final buffer (25 mM Tris, pH 8.0, 250 mM NaCl, 2 mM TCEP). For NMR fragment screening, full length His-tagged human KHK was used as is. For KHK inhibition assays the His-tag was removed by thrombin digestion using biotinylated thrombin, and final cleanup was done through streptavidin agarose resin followed by dialysis in storage buffer (50 mM HEPES, pH 7.5, 250 mM NaCl, 2 mM TCEP). Final protein sequence was confirmed by mass spectrometry. For SPR studies, full length thrombin-cleaved human KHK was chemically biotinylated for immobilization. Sulfo-NHS-LC-LC-biotin was incubated with the protein solution in the presence of ATP analog AMP-PNP to protect the active site during biotinylation. Buffer exchange was done by successive passes through 10k MWCO centricon filter until five full exchanges were accomplished. Protein concentration was monitored throughout and approximately 80% of the starting material was recovered after biotinylation and cleanup.

**NMR fragment screening**. Full length His-tagged KHK was screened against a proprietary 2592 member fragment library using 1D Saturation Transfer Difference (NMR-STD) spectroscopy in NMR. Fragment screen for KHK was carried out using 5 μM protein in 50 mM deuterated Tris-d, 100 mM NaCl, 2 mM deuterated TCEP-d, 5% deuterated glycerol-d at pH 7.5

at 298 K. AMP-PMP 240 μM was used as a positive control in NMR-STD experiments. Standard conditions were run for the NMR-STD method including NS=512. Library compounds were run in either mixtures of 10 or 4 at a final concentration of 240 μM. The 1D STD NMR experiment was carried out using a Bruker Avance 600 MHz NMR spectrometer equipped 1.7 mm cyroprobe at 298K. In the STD experiment, a cascade of sixty 50 ms gaussian shaped (gaus1.1000) pulses were applied for on resonance saturation -2360 Hz from the carrier and applied for off resonance saturation -14819 Hz from the carrier for a total saturation time of 3 sec. Each 50 ms shaped pulse was applied at a power level of $3.16 \times 10^{-4}$ W (35 db) and was followed by a 20 ms delay . In the STD experiment, a 3.0 sec gauss shaped pulse was applied for on resonance saturation -2360 Hz from the carrier and applied for off resonance saturation -14819 Hz from the carrier. Positive signals in the difference spectra indicate ligand binding and the identification of the bound ligand in the mixture was determined by comparison to 1D $^{1}$H reference NMR spectra of each fragment. Data was analyzed using an internal software package.

**Surface plasmon resonance experiments**. Experiments were performed on a Fujifilm AP-3000 instrument. Full length biotinylated KHK was captured onto a SA-101 Fujifilm sensor stick to levels ranging from 7000-8000 RU. Compound binding experiments were performed in 50 mM HEPES pH 7.4, 150 mM NaCl, 0.01% P20, 500 μM TCEP and 3% DMSO at 25 °C. Binding responses were processed using Spotfire software (TIBCO) to zero, x-align, double reference and correct for excluded volume effects of DMSO in the data.

Experiments were carried out for 11 compound concentrations with 2 fold dilutions and a top compound concentration of 300 μM. Compound samples are injected in a stop-flow fashion to allow 60 seconds association and at least 120 seconds dissociation with a blank buffer injection. Equilibrium dissociation constant ($K_D$) was determined using a steady-state affinity algorithm.

**X-ray Crystallography.** Recombinant hKHK was purified and crystallized following protocols described in the literature.[14b, 14d] Apo crystals were soaked for 3 h in solutions containing 25 mM compound in crystal soaking buffer. Compound-bound crystals were then isolated and snap frozen in liquid nitrogen prior to X-ray data collection. X-ray diffraction data were collected at 100 K with radiation of wavelength 1 Å at beamline 17-ID of the Advanced Photon Source at Argonne, on a Pilatus-6M detector. Data were processed using autoPROC[28] with XDS[29] for data integration and the program Scala from the CCP4 Suite[30] for merging and scaling. The structures are isomorphous with PDB entry 3NBV (14d), so phasing was done by rigid body refinement of the protein model from 3NBV. Refinement was carried out using autoBUSTER,[31] while model building and visualization used Coot.[32] Data collection and refinement statistics are given in Table S2.

**In vitro human and rat KHK inhibition assay**. KHK takes ATP and phosphorylates fructose to fructose-1-phosphate, and activity was measured by coupling ADP production to pyruvate kinase-lactate dehydrogenase system with stoichiometric decrease in NADH absorbance at 340 nm. The assay was set up in a 384-well UV plate monitored in continuous mode at room temperature. Compounds were prepared in DMSO as a 40x stock solution and serially diluted using an 11-point scheme on a Biomek FX (Beckman Coulter). One microliter of each compound dilution was transferred to the assay plate, and incubated at room temperature for 30 minutes with reaction mixture containing Assay Buffer (50 mM HEPES, pH 7.4, 140 mM KCl, 3.5 mM $MgCl_2$, 2 mM TCEP, 0.01% Triton X-100), 0.8 mM fructose, 0.8 mM phosphoenol pyruvate, 0.7 mM NADH, 30 U/mL pyruvate kinase-lactate dehydrogenase (Sigma P0294), and 10 nM purified KHK. The reaction was initiated with the addition of 0.2 mM ATP, and the absorbance was measured in kinetic mode at 340 nm for 30 minutes on a SpectraMax reader

(Molecular Devices). The concentrations provided are based on a final reaction volume of 40 μL.

A 2 μM final concentration of compound **8** reported by Maryanoff et al.[14b] was used as hundred percent effect (HPE) control, and 2.5% DMSO which was present in all reaction wells was used as zero percent effect (ZPE) control. Percent inhibition was calculated using the above controls and plotted as a function of compound concentration to generate the concentration response curve, and $IC_{50}$ was calculated on GraphPad PRISM based on the nonlinear fit of the log-transformed data.

**Animal Experimental Methods**. For these studies male Sprague Dawley rats (~200 g body weight) were ordered from Charles River. All animals were acclimated for one week prior to study and fed PicoLab® Rodent Diet 20 ad libitum. For the study in which hepatic and renal F1P was measured, rats with a jugular vein cannula were ordered. For all studies, rats were fasted overnight for 16 hours before beginning the experiment. The morning of the study measuring F1P in hepatic and renal tissue, rats were administered the indicated oral dose of compound **12** formulated as a 10 mL/kg 0.5% methylcellulose nano-milled suspension. One hour following dose, rats received an i.v. 10 mL/kg bolus of fructose (500 mg/kg over 20 seconds). Two minutes following i.v. infusion, rats were euthanized by decapitation and the liver and kidneys were rapidly removed and snap-frozen in liquid nitrogen. Tissues were analyzed by LC/MS for F1P as indicated below. Non-cannulated rats were used for the study measuring changes in plasma fructose study. Animals were administered with the indicated oral dose of compound **12** formulated as a 10 mL/kg 0.5% methylcellulose nano-milled suspension. Blood was collected into $K_2$EDTA coated tubes via tail vein. Plasma was collected following centrifugation according to manufacturer's recommendations. All samples were stored at -80 °C until processing.

**Liver and Kidney Fructose-1-phosphate (F1P) measurements.** Livers and kidneys were rapidly pulverized with a hammer on an aluminum block cooled in liquid nitrogen, ensuring the tissue remained frozen throughout the pulverization. Approximately 100 mg of tissue was aliquoted into a liquid nitrogen cooled 2 mL Lysing Matrix D tube. The tissue weight was determined and then suspended in homogenization buffer, 10 mM ammonium acetate with 10 mM ethylenediaminetetraacetic acid (EDTA), pH 8 solution containing 3 μM xylitol-$^{13}C_5$ as an internal standard. Samples were lysed using a FastPrep 24 vendor at 4 °C, for 40 seconds. Samples were centrifuged at 4 °C, 12,000 RPM for 10 minutes. Supernatant (125 μL) was transferred to a 1.5 mL Eppendorf tube containing 250 μL of mass spectroscopy grade water and centrifuged at 12,000 RPM for 5 minutes. Supernatant was transferred to a 96 deep-well plate and sealed until ready for analysis. All samples were stored at -80 °C until processing.

The quantity of F1P in the samples was determined by analysis LC/MS$^2$ on a QTRAP5500 (ABSciex) coupled with Acquity UPLC (Waters) following the MRM transition of 259 ->97 with following mass spec settings: curtain gas: 35, collision gas: medium, ion spray voltage: -4500 V, temperature: 700 °C, ion source gas 1: 40, ion source gas 2: 60, de-clustering potential: -47, entrance potential: -13.75, collision energy: -20.9, collision cell exit potential: -16.8.

The separation of F1P from other sugar phosphates was achieved by using Shodex RSpak JJ-50 2D PEEK column (2 X 150 mm) with isocratic flow of 10% acetonitrile, 90% water, 20 mM triethyl ammonium acetate, with pH adjusted to 5.8. In each sample, the relative concentration of F1P was quantified by integrating its retention peak and corrected against peak integration of the internal standard 1 μM xylitol-$^{13}C_5$ (after the 1:3 dilution described above)

with a correction ratio or fit into F1P standard curve. The standard curve was generated from spiking various concentrations of F1P in pooled metabolite extracts of tissue homogenates from animals fed a regular diet.

**Measurements of plasma fructose.** Blood was collected and transferred to BD Microtainer tubes coated with $K_2$EDTA, centrifuged at 4 °C and the plasma transferred to a 96-well microtitre plate and stored at -80 °C until analysis. Fructose was extracted from plasma using nine equivalents of extraction solution (80% methanol, 20% 10 mM ammonium acetate with 10 mM EDTA, pH 8 solution containing internal standards (60 μM fructose-$^{13}C_6$). The extracts were centrifuged at 14,000 × g at 4 °C. The supernatant was transferred into a 96 deep-well plate and further diluted with 2 equivalents liquid chromatography-mass spectroscopy grade water.

Prepared plasma samples were subjected to liquid chromatography-mass spectroscopy/mass spectroscopy analysis. Sugar separation was achieved using hydrophilic interaction chromatography (Asahipak NH2P-50 4E, 4.6 x 250 mm) under isocratic elution condition with 0.8 mL/min flow rate using 75% acetonitrile, 25% water containing 5 mM ammonium acetate, pH 9.2. QTRAP5500 (Sciex, MA) Mass Spectrometry source parameter was set as the following: Curtain gas: 35, IonSpray Voltage: -4500, Temperature: 650 °C, Ion source gas 1: 65, Ion source gas 2: 60. MRM transitions for quantitation are set as the following, fructose/glucose: Q1 (179) → Q3 (89), fructose-13C6/glucose-13C6: Q1 (185) → Q3 (92), sorbitol: Q1 (181) → Q3 (89), sorbitol-13C6: Q1 (187) → Q3 (92). The analyte peak of interest was integrated using MultiQuan (Sciex) and converted into a concentration using a stable isotope labeled internal

standard by the following equation: (Analyte peak area)/(fructose-$^{13}C_6$ peak area) × concentration of the fructose-$^{13}C_6$.

ASSOCIATED CONTENT

**Supporting Information**

The following files are available free of charge.

Molecular formula strings, crystal structure describing the environment of Asp27(B) at the interface of the two KHK monomers, distribution of properties for fragment selection among confirmed hits, map of interactions for crystal structure of compound **12**, in vitro selectivity data for compound **12**, data collection and refinement statistics for crystal structures of compounds **3**, **4**, **5**, **7**, **8** and **12** (PDF).

AUTHOR INFORMATION

**Corresponding Author**

*K.H. email: Kim.Huard@Pfizer.com

**Present Addresses**

†K.A. address: Molecular and cellular pharmacology, 1400 McKean Road, Spring House, PA 19477, Janssen Research and development

**Funding Sources**

The research reported in this manuscript was funded by Pfizer. All authors were employed by Pfizer during the completion and analysis of the experiments herein reported. Use of the IMCA-CAT beamline 17-ID at the Advanced Photon Source was supported by the companies of the Industrial Macromolecular Crystallography Association through a contract with Hauptman-

Woodward Medical Research Institute. Use of the Advanced Photon Source was supported by the U.S. Department of Energy, Office of Science, Office of Basic Energy Sciences, under Contract No. DE-AC02-06CH11357

ACKNOWLEDGMENT

The authors would like to thank David Hepworth, Kevin Beaumont and Neal Sach for their contributions to the work reported here and the preparation of the manuscript.

ABBREVIATIONS

KHK, ketohexokinase; F1P, fructose-1-phosphate; hKHK, human KHK; NAFLD, non-alcoholic fatty liver disease; ChREBP, carbohydrate response element binding protein; VLDL, very low density lipoprotein; HTS, high throughput screening; PK, pharmacokinetic; rKHK, rat KHK; FBDD, fragment-based drug discovery; BAP, biotin acceptor peptide; NMR, nuclear magnetic resonance; SPR, surface plasmon resonance; DMSO; dimethylsulfoxide; STD, saturation transfer difference; MW, molecular weight; FQ, fit quality; HLM, human liver microsomes; SFLogD, shake-flask LogD; $P_{app}$, apparent permeability; Fu, fraction unbound in plasma; DOSS, dioctyl sulfosuccinate; RLM, rat liver microsomes; i.v., intravenous; hERG, human ether-a-gogo; CYP450s, cytochrome P450s; LC/MS, liquid chromatography-mass spectrometry; G6P, glucose-6-phosphate; F6P, fructose-6-phosphate; G1P, glucose-1-phosphate; DBU, 1,8-diazabicyclo[5.4.0]indec-7-ene; $POCl_3$, phosphoryl chloride; MTBE, methyl tert-butyl ether.

**Accession Codes**

Atomic coordinates and structure factors for hKHK bound to compounds **3**, **4**, **5**, **7**, **8** and **12** have been deposited to the RCSB, with PDB ID codes 5WBM, 5WBO, 5WBP, 5WBQ, 5WBR

and 5WBZ respectively. Authors will release the atomic coordinates and experimental data upon article publication.

REFERENCES

1. Bonthron, D. T.; Brady, N.; Donaldson, I. A.; Steinmann, B. Molecular basis of essential fructosuria: molecular cloning and mutational analysis of human ketohexokinase (fructokinase). *Hum. Mol. Genet.* **1994,** *3*, 1627-1631.

2. Asipu, A.; Hayward, B. E.; O'Reilly, J.; Bonthron, D. T. Properties of normal and mutant recombinant human ketohexokinases and implications for the pathogenesis of essential fructosuria. *Diabetes* **2003,** *52*, 2426-2432.

3. Ishimoto, T.; Lanaspa, M. A.; Le, M. T.; Garcia, G. E.; Diggle, C. P.; Maclean, P. S.; Jackman, M. R.; Asipu, A.; Roncal-Jimenez, C. A.; Kosugi, T.; Rivard, C. J.; Maruyama, S.; Rodriguez-Iturbe, B.; Sanchez-Lozada, L. G.; Bonthron, D. T.; Sautin, Y. Y.; Johnson, R. J. Opposing effects of fructokinase C and A isoforms on fructose-induced metabolic syndrome in mice. *Proc. Natl. Acad. Sci. U. S. A.* **2012,** *109*, 4320-4325.

4. (a) Jin, R.; Vos, M. B. Fructose and liver function--is this behind nonalcoholic liver disease? *Curr. Opin. Clin. Nutr. Metab. Care* **2015,** *18*, 490-495; (b) Schultz, A.; Neil, D.; Aguila, M. B.; Mandarim-de-Lacerda, C. A. Hepatic adverse effects of fructose consumption independent of overweight/obesity. *Int. J. Mol. Sci.* **2013,** *14*, 21873-21886; (c) Sun, S. Z.; Empie, M. W. Fructose metabolism in humans - what isotopic tracer studies tell us. *Nutr. Metab.* **2012,** *9*, 89; (d) Abdelmalek, M. F.; Suzuki, A.; Guy, C.; Unalp-Arida, A.; Colvin, R.; Johnson, R. J.; Diehl, A. M.; Nonalcoholic Steatohepatitis Clinical Research, N. Increased fructose consumption is associated with fibrosis severity in patients with nonalcoholic fatty liver disease. *Hepatology* **2010,** *51*, 1961-1971; (e) Ouyang, X.; Cirillo, P.; Sautin, Y.; McCall, S.; Bruchette,

J. L.; Diehl, A. M.; Johnson, R. J.; Abdelmalek, M. F. Fructose consumption as a risk factor for non-alcoholic fatty liver disease. *J. Hepatol.* **2008,** *48*, 993-999.

5. (a) Softic, S.; Cohen, D. E.; Kahn, C. R. Role of dietary fructose and hepatic de novo lipogenesis in fatty liver disease. *Dig. Dis. Sci.* **2016,** *61*, 1282-1293; (b) Herman, M. A.; Samuel, V. T. The sweet path to metabolic demise: fructose and lipid synthesis. *Trends Endocrinol. Metab.* **2016,** *27*, 719-730; (c) Kim, M. S.; Krawczyk, S. A.; Doridot, L.; Fowler, A. J.; Wang, J. X.; Trauger, S. A.; Noh, H. L.; Kang, H. J.; Meissen, J. K.; Blatnik, M.; Kim, J. K.; Lai, M.; Herman, M. A. ChREBP regulates fructose-induced glucose production independently of insulin signaling. *J. Clin. Invest.* **2016,** *126*, 4372-4386.

6. Erion, D. M.; Popov, V.; Hsiao, J. J.; Vatner, D.; Mitchell, K.; Yonemitsu, S.; Nagai, Y.; Kahn, M.; Gillum, M. P.; Dong, J.; Murray, S. F.; Manchem, V. P.; Bhanot, S.; Cline, G. W.; Shulman, G. I.; Samuel, V. T. The role of the carbohydrate response element-binding protein in male fructose-fed rats. *Endocrinology* **2013,** *154*, 36-44.

7. (a) Stanhope, K. L.; Medici, V.; Bremer, A. A.; Lee, V.; Lam, H. D.; Nunez, M. V.; Chen, G. X.; Keim, N. L.; Havel, P. J. A dose-response study of consuming high-fructose corn syrup-sweetened beverages on lipid/lipoprotein risk factors for cardiovascular disease in young adults. *Am. J. Clin. Nutr.* **2015,** *101*, 1144-1154; (b) Stanhope, K. L.; Schwarz, J. M.; Keim, N. L.; Griffen, S. C.; Bremer, A. A.; Graham, J. L.; Hatcher, B.; Cox, C. L.; Dyachenko, A.; Zhang, W.; McGahan, J. P.; Seibert, A.; Krauss, R. M.; Chiu, S.; Schaefer, E. J.; Ai, M.; Otokozawa, S.; Nakajima, K.; Nakano, T.; Beysen, C.; Hellerstein, M. K.; Berglund, L.; Havel, P. J. Consuming fructose-sweetened, not glucose-sweetened, beverages increases visceral adiposity and lipids and decreases insulin sensitivity in overweight/obese humans. *J. Clin. Invest.* **2009,** *119*, 1322-1334.

8. (a) Lustig, R. H.; Mulligan, K.; Noworolski, S. M.; Tai, V. W.; Wen, M. J.; Erkin-Cakmak, A.; Gugliucci, A.; Schwarz, J. M. Isocaloric fructose restriction and metabolic improvement in children with obesity and metabolic syndrome. *Obesity* **2016,** *24*, 453-460; (b) Schwarz, J. M.; Noworolski, S. M.; Wen, M. J.; Dyachenko, A.; Prior, J. L.; Weinberg, M. E.; Herraiz, L. A.; Tai, V. W.; Bergeron, N.; Bersot, T. P.; Rao, M. N.; Schambelan, M.; Mulligan, K. Effect of a high-fructose weight-maintaining diet on lipogenesis and liver fat. *J. Clin. Endocrinol. Metab.* **2015,** *100*, 2434-2442.

9. (a) Abid, A.; Taha, O.; Nseir, W.; Farah, R.; Grosovski, M.; Assy, N. Soft drink consumption is associated with fatty liver disease independent of metabolic syndrome. *J. Hepatol.* **2009,** *51*, 918-924; (b) Assy, N.; Nasser, G.; Kamayse, I.; Nseir, W.; Beniashvili, Z.; Djibre, A.; Grosovski, M. Soft drink consumption linked with fatty liver in the absence of traditional risk factors. *Can. J. Gastroenterol.* **2008,** *22*, 811-816.

10. Ishimoto, T.; Lanaspa, M. A.; Rivard, C. J.; Roncal-Jimenez, C. A.; Orlicky, D. J.; Cicerchi, C.; McMahan, R. H.; Abdelmalek, M. F.; Rosen, H. R.; Jackman, M. R.; MacLean, P. S.; Diggle, C. P.; Asipu, A.; Inaba, S.; Kosugi, T.; Sato, W.; Maruyama, S.; Sanchez-Lozada, L. G.; Sautin, Y. Y.; Hill, J. O.; Bonthron, D. T.; Johnson, R. J. High-fat and high-sucrose (western) diet induces steatohepatitis that is dependent on fructokinase. *Hepatology* **2013,** *58*, 1632-1643.

11. Lanaspa, M. A.; Ishimoto, T.; Li, N.; Cicerchi, C.; Orlicky, D. J.; Ruzycki, P.; Rivard, C.; Inaba, S.; Roncal-Jimenez, C. A.; Bales, E. S.; Diggle, C. P.; Asipu, A.; Petrash, J. M.; Kosugi, T.; Maruyama, S.; Sanchez-Lozada, L. G.; McManaman, J. L.; Bonthron, D. T.; Sautin, Y. Y.; Johnson, R. J. Endogenous fructose production and metabolism in the liver contributes to the development of metabolic syndrome. *Nat. Commun.* **2013,** *4*, 2434.

12. Sachs, B.; Sternfeld, L.; Kraus, G. Essential fructosuria: Its pathophysiology. *Am. J. Dis. Child.* **1942,** *63*, 252-269.

13. Bais, R.; James, H. M.; Rofe, A. M.; Conyers, R. A. The purification and properties of human liver ketohexokinase. A role for ketohexokinase and fructose-bisphosphate aldolase in the metabolic production of oxalate from xylitol. *Biochem. J.* **1985,** *230*, 53-60.

14. (a) Trinh, C. H.; Asipu, A.; Bonthron, D. T.; Phillips, S. E. V. Structures of alternatively spliced isoforms of human ketohexokinase. *Acta Crystallogr., Sect. D: Biol. Crystallogr.* **2009,** *65*, 201-211, S201/201; (b) Maryanoff, B. E.; O'Neill, J. C.; McComsey, D. F.; Yabut, S. C.; Luci, D. K.; Jordan, A. D.; Masucci, J. A.; Jones, W. J.; Abad, M. C.; Gibbs, A. C.; Petrounia, I. Inhibitors of ketohexokinase: discovery of pyrimidinopyrimidines with specific substitution that complements the ATP-binding site. *ACS Med. Chem. Lett.* **2011,** *2*, 538-543; (c) Maryanoff, B. E.; O'Neill, J. C.; McComsey, D. F.; Yabut, S. C.; Luci, D. K.; Gibbs, A. C.; Connelly, M. A. Pyrimidinopyrimidine inhibitors of ketohexokinase: Exploring the ring C2 group that interacts with Asp-27B in the ligand binding pocket. *Bioorg. Med. Chem. Lett.* **2012,** *22*, 5326-5329; (d) Gibbs, A. C.; Abad, M. C.; Zhang, X.; Tounge, B. A.; Lewandowski, F. A.; Struble, G. T.; Sun, W.; Sui, Z.; Kuo, L. C. Electron density guided fragment-based lead discovery of ketohexokinase inhibitors. *J. Med. Chem.* **2010,** *53*, 7979-7991; (e) Abad, M. C.; Gibbs, A. C.; Zhang, X. Electron density guided fragment-based drug design-a lead generation example. *Methods Enzymol.* **2011,** *493*, 487-508; (f) Zhang, X.; Song, F.; Kuo, G.-H.; Xiang, A.; Gibbs, A. C.; Abad, M. C.; Sun, W.; Kuo, L. C.; Sui, Z. Optimization of a pyrazole hit from FBDD into a novel series of indazoles as ketohexokinase inhibitors. *Bioorg. Med. Chem. Lett.* **2011,** *21*, 4762-4767.

15. (a) Lanter, J.; Zhang, X.; Sui, Z. Medicinal chemistry inspired fragment-based drug discovery. *Methods Enzymol.* **2011,** *493*, 421-445; (b) Johnson, C. N.; Erlanson, D. A.; Murray, C. W.; Rees, D. C. Fragment-to-Lead Medicinal Chemistry Publications in 2015. *J. Med. Chem.* **2017,** *60*, 89-99.

16. Lau, W. F.; Withka, J. M.; Hepworth, D.; Magee, T. V.; Du, Y. J.; Bakken, G. A.; Miller, M. D.; Hendsch, Z. S.; Thanabal, V.; Kolodziej, S. A.; Xing, L.; Hu, Q.; Narasimhan, L. S.; Love, R.; Charlton, M. E.; Hughes, S.; Hoorn, W. P.; Mills, J. E. Design of a multi-purpose fragment screening library using molecular complexity and orthogonal diversity metrics. *J. Comput.-Aided Mol. Des.* **2011,** *25*, 621-636.

17. Lee, K. L.; Ambler, C. M.; Anderson, D. R.; Boscoe, B. P.; Bree, A. G.; Brodfuehrer, J. I.; Chang, J. S.; Choi, C.; Chung, S.; Curran, K. J.; Day, J. E.; Dehnhardt, C. M.; Dower, K.; Drozda, S. E.; Frisbie, R. K.; Gavrin, L. K.; Goldberg, J. A.; Han, S.; Hegen, M.; Hepworth, D.; Hope, H. R.; Kamtekar, S.; Kilty, I. C.; Lee, A.; Lin, L.-L.; Lovering, F. E.; Lowe, M. D.; Mathias, J. P.; Morgan, H. M.; Murphy, E. A.; Papaioannou, N.; Patny, A.; Pierce, B. S.; Rao, V. R.; Saiah, E.; Samardjiev, I. J.; Samas, B. M.; Shen, M. W. H.; Shin, J. H.; Soutter, H. H.; Strohbach, J. W.; Symanowicz, P. T.; Thomason, J. R.; Trzupek, J. D.; Vargas, R.; Vincent, F.; Yan, J.; Zapf, C. W.; Wright, S. W. Discovery of clinical candidate 1-{[(2S,3S,4S)-3-ethyl-4-fluoro-5-oxopyrrolidin-2-yl]methoxy}-7-methoxyisoquinoline-6-carboxamide (PF-06650833), a potent, selective inhibitor of interleukin-1 receptor associated kinase 4 (IRAK4), by fragment-based drug design. *J. Med. Chem.* **2017,** *60*, 5521-5542.

18. Mayer, M.; Meyer, B. Characterization of ligand binding by saturation transfer difference NMR spectroscopy. *Ang. Chem. Int. Ed.* **1999,** *38*, 1784-1788.

19. Reynolds, C. H.; Tounge, B. A.; Bembenek, S. D. Ligand binding efficiency: trends, physical basis, and implications. *J. Med. Chem.* **2008,** *51*, 2432-2438.

20. Obach, R. S. The prediction of human clearance from hepatic microsomal metabolism data. *Curr. Opin. Drug Discovery Dev.* **2001,** *4*, 36-44.

21. Hay, T.; Jones, R.; Beaumont, K.; Kemp, M. Modulation of the partition coefficient between octanol and buffer at pH 7.4 and pKa to achieve the optimum balance of blood clearance and volume of distribution for a series of tetrahydropyran histamine type 3 receptor antagonists. *Drug. Metab. Dispos.* **2009,** *37*, 1864-1870.

22. Di, L.; Whitney-Pickett, C.; Umland, J. P.; Zhang, H.; Zhang, X.; Gebhard, D. F.; Lai, Y.; Federico, J. J., 3rd; Davidson, R. E.; Smith, R.; Reyner, E. L.; Lee, C.; Feng, B.; Rotter, C.; Varma, M. V.; Kempshall, S.; Fenner, K.; El-Kattan, A. F.; Liston, T. E.; Troutman, M. D. Development of a new permeability assay using low-efflux MDCKII cells. *J. Pharm. Sci.* **2011,** *100*, 4974-4985.

23. Banker, M. J.; Clark, T. H.; Williams, J. A. Development and validation of a 96-well equilibrium dialysis apparatus for measuring plasma protein binding. *J. Pharm. Sci.* **2003,** *92*, 967-974.

24. Zonouzi, A.; Izakian, Z.; Ng, S. W. Novel synthesis of some new fluorescent 2-amino-3-cyanopyridines. *Heterocycles* **2012,** *85*, 2713-2721.

25. Ishikawa, N.; Sasaki, S. Preparation of perfluoroalkylated benzoheterocyclic compounds using hexafluoro-1,2-epoxypropane. *Bull. Chem. Soc. Jpn.* **1977,** *50*, 2164-2167.

26. Bagal, S. K.; Cui, J. J.; Greasley, S. E.; Lunney, E. A.; McAlpine, I. J.; Nagata, A.; Ninkovic, S.; Omoto, K.; Skerratt, S. E.; Storer, R. I.; Warmus, J. S. N-Pyrazolyl

Pyridinylbenzamides as Tropomyosin-related Kinase Inhibitors and Their Preparation. WO2015170218A1, 2015.

27. Gangjee, A.; Li, W.; Yang, J.; Kisliuk, R. L. Design, synthesis, and biological evaluation of classical and nonclassical 2-amino-4-oxo-5-substituted-6-methylpyrrolo[3,2-d]pyrimidines as dual thymidylate synthase and dihydrofolate reductase inhibitors. *J. Med. Chem.* **2008,** *51*, 68-76.

28. Vonrhein, C.; Flensburg, C.; Keller, P.; Sharff, A.; Smart, O.; Paciorek, W.; Womack, T.; Bricogne, G. Data processing and analysis with the autoPROC toolbox. *Acta Crystallogr., Sect. D: Biol. Crystallogr.* **2011,** *67*, 293-302.

29. Kabsch, W. Xds. *Acta Crystallogr., Sect. D: Biol. Crystallogr.* **2010,** *66*, 125-132.

30. Winn, M. D.; Ballard, C. C.; Cowtan, K. D.; Dodson, E. J.; Emsley, P.; Evans, P. R.; Keegan, R. M.; Krissinel, E. B.; Leslie, A. G. W.; McCoy, A.; McNicholas, S. J.; Murshudov, N.; Pannu, N. S.; Potterton, E. A.; Powell, H. R.; Read, R. J.; Vagin, A.; Wilson, K. S. Overview of the CCP4 suite and current developments. *Acta Crystrallogr., Sect. D: Biol. Crystallogr.* **2011,** *67*, 235-242.

31. Bricogne, G.; Blanc, E.; Brandl, M.; Flensburg, C.; Keller, P.; Paciorek, W.; Roversi, P.; Sharff, A.; Smart, O. S.; Vonrhein, C.; Womack, T. O. *BUSTER version X.Y.Z*. Cambridge, United Kingdom: Global Phasing Ltd 2016.

32. Emsley, P.; Lohkamp, B.; Scott, W. G.; Cowtan, K. Features and development of Coot. *Acta Crystallogr., Sect. D: Biol. Crystallogr.* **2010,** *66*, 486-501.

Graphic TOC

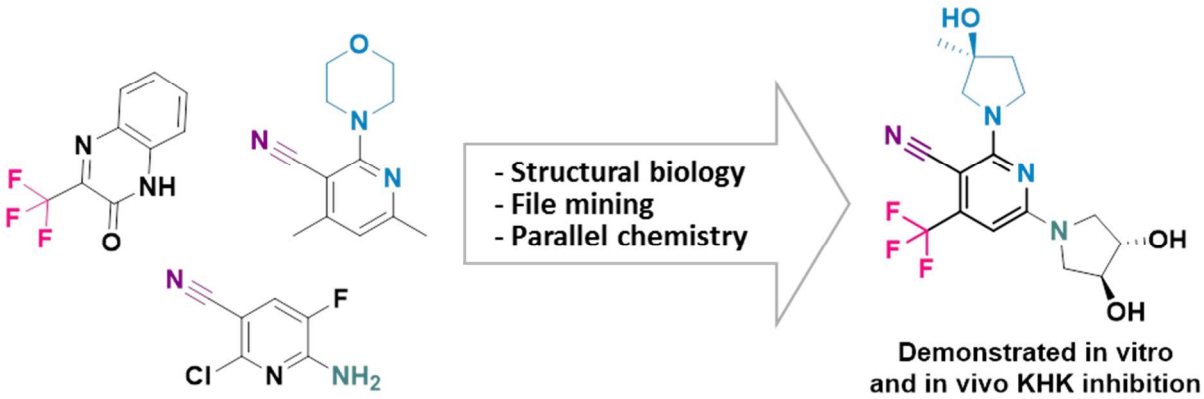
- Structural biology
- File mining
- Parallel chemistry
Demonstrated in vitro
and in vivo KHK inhibition